CaO-BASED ADSORBENT FOR CO_2 CAPTURE: KINETIC STUDY

LAW SER CHYEN

A project report submitted in partial fulfilment of the requirements for the award of Bachelor of Engineering (Hons.) Chemical Engineering

Lee Kong Chian Faculty of Engineering and Science
Universiti Tunku Abdul Rahman

September 2018

DECLARATION

I hereby declare that this project report is based on my original work except for citations and quotations which have been duly acknowledged. I also declare that it has not been previously and concurrently submitted for any other degree or award at UTAR or other institutions.

Signature : _____

Name : Law Ser Chyen

ID No. : 14UEB07182

Date : 18/9/2018

APPROVAL FOR SUBMISSION

I certify that this project report entitled **"CaO-BASED ADSORBENT FOR CO_2 CAPTURE: KINETIC STUDY"** was prepared by **LAW SER CHYEN** has met the required standard for submission in partial fulfilment of the requirements for the award of Bachelor of Engineering (Hons.) Chemical Engineering at Universiti Tunku Abdul Rahman.

Approved by,

Signature : _____

Supervisor : Dr. Lee Zhi Hua

Date : 18/9/2018

ACKNOWLEDGEMENTS

I would like to thank everyone who had contributed to the successful completion of this project. I would like to express my gratitude to my research supervisor, Dr. Lee Zhi Hua for her invaluable advice, guidance and her enormous patience throughout the development of the research.

In addition, I would also like to express my gratitude to my loving parents and friends who had helped and given me encouragement during my hard times. I would like to specially thanks Miss Vitiyaa a/p Selva Kumar for helping and supporting me throughout my project. Without their guidance and knowledge, this research would have not come to completion.

ABSTRACT

Since the first industrial revolution, production of carbon dioxide as industrial by-product is inevitable. Carbon capture storage (CCS) technology which involves carbonation of carbon dioxide into calcium carbonate with the aid of calcium oxide adsorbent is widely applied. It is known that, addition of nickel oxide as catalyst is able to lower the carbonation temperature, which will lower the energy consumption required to raise the flue gas to desired temperature in order for the reaction to take place, thus leads to lower energy penalty for high flow fossil fuel plant. During this project, calcium oxide and calcium oxide-nickel oxide adsorbents were successfully synthesised through sol-gel method. The data needed for this analysis was obtained from carbonation of adsorbents at temperatures of 400, 500 and 600 ºC with the aid of Thermogravimetric Analyser (TGA). The results showed that high adsorption rate and adsorption capacity could be achieved at the initial stage, chemical reaction-controlled stage, at higher carbonation temperature as well as by addition of NiO catalyst. CaO-NiO adsorbent carbonated at 600 ºC was able to achieve high adsorption capacity of 0.5661 mg CO_2/ mg CaO as well as high adsorption rate of 0.3533 mg CO_2/ mg CaO.min. Kinetic study of calcium oxide-based adsorbent for carbon dioxide capture had been conducted by using isothermal analysis method. It was found that, the addition of NiO catalyst caused decrease in activation energy, *E* for transition stage and diffusion-controlled stage as well as increased pre-exponential factor, *A* for chemical reaction-controlled stage. Besides, characterisation of adsorbents was carried out by means of Scanning Electron Microscope (SEM) to study the surface morphology, Energy Dispersive X-ray Spectroscopy (EDX) was used to investigate the distribution of different elements and X-ray diffraction (XRD) was used to understand the crystalline structure.

TABLE OF CONTENTS

LIST OF TABLES

LIST OF FIGURES

LIST OF SYMBOLS / ABBREVIATIONS

$\left(\frac{d\alpha}{dt}\right)_{\alpha}$	degree of conversion, min^{-1}
A	pre-exponential factor, min^{-1}
A_{α}	apparent pre-exponential factor, min^{-1}
d_x	Crystallite size, nm
E	activation energy, J mol^{-1}
E_{α}	apparent activation energy, J mol^{-1}
f_{CaO}	mass fraction of CaO in adsorbent
$FWHM$	Full Width at Half Maximum, rad
$g(\alpha)$	integral form of the reaction model
$k(T)$	function of rate constant, min^{-1}
k_c	rate constant for chemical-controlled stage
k_d	rate constant for diffusion-controlled stage
k_t	rate constant for transition stage
$m(0)$	mass of adsorbent at time 0, mg
$m(t)$	mass of adsorbent at time t, mg
n	order of reaction
R	universal ideal gas constant, J mol^{-1} K^{-1}
t	time, min
T	temperature, K
T_0	initial temperature, K
α	conversion of adsorbent
β	heating rate, K/min
θ	angle, °
θ	Bragg angle, rad
λ	wavelength of X−ray, nm

$CaCO_3$	calcium carbonate
CaO	calcium oxide
CaO-NiO	calcium oxide-nickel oxide
CO_2	carbon dioxide

CCS	carbon capture and storage
CLP	calcium looping process
CR	Coats-Redfern
FWO	Flynn–Wall–Ozawa
GHGs	greenhouse gasses
KAS	Kissenger–Akahira–Sunose
SEM-EDX	Scanning Electron Microscope - Energy Dispersive X-ray Analyzer
TGA	Thermogravimetric Analyser
UNFCCC	United Nations Framework Convention on Climate Change
XRD	X-ray diffraction

LIST OF APPENDICES

CHAPTER 1

INTRODUCTION

1.1 General Introduction

Since the first industrial revolution, the concentration of greenhouse gasses (GHGs) in the atmosphere has been going uphill. There are several GHGs in the atmosphere including methane, ozone, nitrous oxide, carbon dioxide (CO_2) and fluorinated gases. CO_2 is considered as one of the major GHGs as it accounts 82 % of all United States GHGs emissions in the year of 2015 (United States Environmental Protection Agency, n.d.). Majority amount of the CO_2 emission are resulting from activities such as burning of fossil fuels as well as deforestation. Despite numerous government policies had been launched to tackle the anthropogenic GHGs emission problem, there are still opportunities for further reduction of GHGs emission.

It is known that increasing CO_2 emission will enhance natural greenhouse effect, thus leads to global warming as well as climate change. This issue has been escalated and several actions had been taken by non-governmental organizations. For instance, the United Nations Framework Convention on Climate Change (UNFCCC) adopted Kyoto Protocol in Japan on 1997. Mandatory limits on GHGs emissions are set for parties that ratified the treaty. Therefore, participating parties assured to maintain low emissions of carbon annually (United Nations Climate Change, n.d.).

The best way to conquer the high CO_2 emission issue is by using renewable energy as replacement for fossil fuel energy. However, it is difficult to substitute fossil fuel energy rapidly as developing renewable energy sources requires huge capital as well as lots of time. Since ceasing the production of CO_2 from burning fossil fuel is impossible in current situation, introduction of carbon capture and storage (CCS) technology is considered as one of the most promising mitigation pathways. It is able to solve high CO_2 emission problem as well as allow the use of fossil fuels energy in this CO_2 emission constrained world (Maroto-Valer, 2010).

CCS is a technology dedicated to mitigate stationary source CO_2 emission problem. This technology is capable of capturing 90 % CO_2 emissions produced from the use of fossil fuel for electricity generation as well as other industrial processes (Carbon Capture & Storage Association, n.d.). Apart from that, it consists of three main parts including, capture, transport and storage of CO_2 (He, et al., 2017).

1.1.1 Existing CO_2 Capture Technologies

Out of the three parts in CCS, CO_2 capture is the most challenging and costly part of this technology as it accounts for 66.67 % of the total cost of the whole technology (Maroto-Valer, 2010). As a result, CO_2 capture is the most widely studied part compared to others. There are several methods available for CO_2 capture, including pre-combustion capture, oxy-combustion capture and post-combustion capture (Sivalingam, 2013).

Pre-combustion capture implies CO_2 is captured before the gas undergoes combustion process. Firstly, fuel is converted into syngas with carbon monoxide and hydrogen. Next, syngas is converted into CO_2 and hydrogen (Budzianowski, 2017). The CO_2 formed is captured, whilst hydrogen and air undergoes combustion without emitting CO_2 to form energy (Kanniche, et al., 2010).

Instead of using air during combustion process, oxy-combustion capture uses oxygen with purity up to 97 % to combust the fuel (Kanniche, et al., 2010). By using high purity oxygen, the flue gas produced consists mainly CO_2 and water which makes CO_2 easier for separation. Condensation of water is sufficient to separate the water from CO_2. One of the limitations of this method is requirement of continuous flow oxygen (Lecomte, et al., 2010).

For post-combustion capture, CO_2 is captured from flue gas produced during combustion of fuel in air. Besides application in power plant, it is commonly used in other industries such as cement, steel or iron plant (Lecomte, et al., 2010). This method is popular as it can be installed into the original process without much alteration of the original plants (Martínez, et al., 2011). The processes involved in this method are solvent absorption, sorbent adsorption, membrane separation and cryogenic distillation (Sivalingam, 2013).

1.1.2 Calcium Looping Process (CLP)

Currently, CLP is one of the mature post-combustion capture technologies being applied around the industry. This method involves a reversible reaction between calcium carbonate and CO_2 with the aid of calcium oxide-based adsorbent as shown in chemical equation 1.1. The forward reaction is carbonation whilst the reverse reaction is calcination.

$$CaO\ (s)\ +\ CO_2\ (g)\ \rightleftharpoons\ CaCO_3\ (s) \qquad (1.1)$$

Firstly, flue gas from fossil-fuel power plant is conveyed into carbonator. In carbonator, CO_2 react with calcium oxide-based adsorbent (CaO-based) to form calcium carbonate at temperature of 650 to 700 °C. Next, the calcium carbonate formed is transferred to calciner for adsorbent regeneration (Chi, et al., 2017). In calciner with temperature between 650 to 900 °C, calcium carbonate broke down into calcium oxide and carbon dioxide (He, et al., 2017). The CO_2 formed can be compressed for storage. The regenerated calcium oxide is sent to carbonator for recycle purpose (Chi, et al., 2017).

1.1.3 Advantages of Calcium Looping Process (CLP)

The raw material, calcium oxide is a natural product. It is non-hazardous and highly available at low prices in the market (Chi, et al., 2017). This method is also known as Calcium Looping Cycle because the reaction is reversible. By having reversible reaction, the calcium oxide can be regenerated from time to time by reverse reaction for reuse purpose. Hence, smaller amount of fresh calcium oxide is required.

Apart from that, carbonator and calciner applied fluidized bed technology with good gas and solid contacting condition (Liu, et al., 2017). Since large scale fluidized bed technology is matured, scaling up of the CLP technology should not be a problem. Besides, CLP is categorized as post-combustion capture method. As mentioned, this type of capture method provides higher flexibility as it is suitable for retrofitting of existing power plant without affecting another unit operation. Hence, lesser time and investment is needed to restructure the original plant.

In ideal conditions, calcium oxide provides high capture capacity of 0.786 g CO_2/ g adsorbent which makes it a suitable material for CO_2 capture (Skoufa, et al., 2016). Besides, CLP technology is well known in having rapid kinetics for carbonation and calcination (Skoufa, et al., 2016). CLP has lower efficiency penalty which is 7 % point whilst, other methods such as amine scrubbing and oxy-combustion technology has efficiency penalty for electricity production of 12.5 % point (Hanak, Anthony and Manovic, 2015).

1.1.4 Disadvantages of Calcium Looping Process (CLP)

Apart from the advantages mentioned, there are several limitations needed to be considered. Firstly, the capital investment for construction of CLP might be high as high thermal power is needed. As mentioned in previous part, fluidized bed reactor is applied. In other words, particle attrition of calcium oxide might be a problem after multiple carbonation-calcination cycles (Hanak, Anthony and Manovic, 2015).

Based on studies, calcium oxide will deteriorate after going through multiple carbonation-calcination cycles. The main reason of calcium oxide deactivation is thermal sintering of the adsorbents. According to (Hanak, Anthony and Manovic, 2015), the deactivation will lead to capacity decrease of 90 mol% within 5 cycles. The capacity decrease is mainly due to the reduction in surface area and volume of pore of calcium oxide (Chi, et al., 2017). Consequently, constant fresh calcium oxide flow is necessary, thus, leading to cost increase of this technology.

1.2 Importance of Study

As mentioned, conventional CLP system has problem in decreased CO_2 capture capacity after several cycles. Thus, it is crucial to modify the existing one to gives high and stable sorption performance (Dunstan, et al., 2016). Based on studies, there are plenty of approaches proposed to overcome the disadvantages mentioned in previous part, including modification of precursors, thermal pre-treatment, hydration pre-treatment and addition of dopants or support on calcium oxide. However, these recommendations are incompatible with industrial production scale (Jing, et al., 2017). For instance, modification of precursors might lead to additional cost during adsorbent preparation (Liu, et al., 2010). Moreover, adsorbent might lose significant CO_2 capture capacity after thermal treatment due to reduction of pore volume (Manovic, Anthony and Loncarevic, 2009). Hence, it is important to develop a more feasible solution to overcome the disadvantages mentioned.

1.3 Problem Statement

Although CLP has much lower energy penalties compared to other methods, there is still room for improvement for this process. For instance, the elevated carbonation temperature is known be the major problem of this process. Normally, the temperature of flue gas released from powerplant is between 100 to 150 °C (Mokhtar, Taib and Hassim, 2014). On the other hand, the temperature needed for CO_2 capture

reaction in carbonation step is between 650 to 700°C. The differences between both temperatures is approximately 500°C. Based on study, approximately 40% additional energy consumption is required to raise the flue gas to desired temperature in order for the reaction to take place, thus leads to high energy penalty for high flow fossil fuel plant (Lee, et al., 2015). Hence, it is crucial to lower the carbonation temperature in order to minimize the energy consumption during CO_2 capture.

It is known that the introduction of first-row transition metal oxides as catalyst into conventional CLP system would lower the optimum temperature needed for carbonation to occur. Out of that row of metal oxides, addition of nickel oxide is known to provide lowest carbonation temperature (Jing, et al., 2017). With the aid of nickel oxide catalyst, the carbonation activation energy can be lowered and thus lower the reaction optimum temperature. However, the kinetic data such as activation energy is yet to be known. Thus, this study aimed to study the kinetic of calcium oxide-nickel oxide for CO_2 capture.

1.4 Aim and Objectives

The aim of this project is to synthesise and study the kinetic of calcium oxide-nickel oxide. The objectives of this project are listed as follows:

(i) To characterise calcium oxide-nickel oxide adsorbent with the aid of Scanning Electron Microscope - Energy Dispersive X-ray Analyzer (SEM-EDX) and X-ray diffraction (XRD).

(ii) To study the carbon dioxide adsorption with the aid of Thermogravimetric Analyser (TGA).

(iii) To study the kinetic of calcium oxide-nickel oxide adsorbent for carbon dioxide capture.

1.5 Scope and Limitation of the Study

In order to achieve the aims and objectives, the following scopes are studied. The weight changes on calcium oxide-nickel oxide adsorbent is studied with the aid of Thermogravimetric Analyser (TGA) at temperature around 450°C. The data obtained from TGA is further processed for kinetics study of calcium oxide-nickel oxide adsorbent. Besides, the effect on characteristic of nickel oxide catalyst and catalytic activity are studied and compared. Characteristics of nickel oxide are studied by

using Scanning Electron Microscope - Energy Dispersive X-ray Analyzer (SEM-EDX) and X-ray diffraction (XRD).

One of the limitations of this study is inability to visualise the actual phenomenon. According to studies, the flue gases exiting from fossil fuelled power plants contains approximately 10-15 mol% of CO_2 and the rest are composed of nitrogen, water and oxygen (Dunstan, et al., 2016). However, in this project, pure CO_2 is used to study the kinetic of calcium oxide-nickel oxide adsorbent. Besides, regeneration of the adsorbent through calcination process is not studied in this project.

1.6 Contribution of the Study

Upon completion of this study, further understanding of the kinetics involved in calcium oxide-nickel oxide adsorbent for CO_2 capture will be achieved. By having this understanding, the optimum temperature for carbonation reaction to occur can be lowered. Hence, the energy consumption required to raise the flue gas to desired temperature can be lowered, thus lower the energy penalty. Besides, lowering the carbonation reaction temperature is able to reduce the thermal sintering problem of adsorbent.

1.7 Outline of the Report

Chapter 1 is introduction which covers the general background of existing CO_2 capture technologies. Besides, importance of study, problem statement, aims and objectives, contribution of the study as well as scope and limitation of the study are elaborated. Chapter 2 is literature review which reviewed different facts and results obtained from various sources that is related to this topic. Besides, useful information and recommendations will be taken note in the report before conducting the research. Chapter 3 involves methodology and work plan whereby the types of materials used, equipment used, summary of research methodology, adsorbent preparation, kinetic study as well as characterization methods were presented. Chapter 4 is results and discussion which embraces the results obtained from TGA, SEM, XRD and BET as well as the kinetic study of calcium oxide-nickel oxide adsorbent based on the process parameters tested. Lastly, chapter 5 is conclusion and recommendations which concludes the study and provides recommendations for future research.

CHAPTER 2

LITERATURE REVIEW

2.1 CO_2 Capture by CaO-Based Adsorbent

Calcium oxide (CaO) adsorbent is derived from limestone which is widely available in nature. It is non-hazardous and highly available at low prices in the market (Chi, et al., 2017). In ideal conditions, it is able to achieve high capture capacity of 0.786 g CO_2/ g CaO which makes it a suitable material for CO_2 capture (Skoufa, et al., 2016). Besides, it is commonly used as adsorbent in Calcium Looping Process (CLP).

CLP comprises the separation of CO_2 with the aid of CaO adsorbent. It involves reversible reaction as shown in chemical equation 2.1 and 2.2 (Sivalingam, 2013).

$$Carbonation: CaO\ (s) + CO_2\ (g) \rightarrow CaCO_3\ (s)\ \ \Delta H = -178\ kJ \qquad (2.1)$$

$$Calcination:\ CaCO_3\ (s) \rightarrow CaO\ (s) +\ CO_2\ (g)\ \ \Delta H = +178\ kJ \qquad (2.2)$$

The forward reaction is carbonation whilst the reverse reaction is calcination. By having reversible reaction, the CaO adsorbent can be regenerated from time to time by reverse reaction for reuse purpose. Hence, smaller amount of fresh calcium oxide is required. In addition, CLP is well known in having rapid kinetics for carbonation and calcination (Skoufa, et al., 2016). It has lower efficiency penalty which is 7 % point whilst, other methods such as amine scrubbing and oxy-combustion technology has efficiency penalty for electricity production of 12.5 % point (Hanak, Anthony and Manovic, 2015).

The working principle of CLP are as follow. Firstly, flue gas contains CO_2 from fossil-fuel power plant undergoes carbonation to form calcium carbonate at temperature between 650°C to 700°C in carbonator. Next, the calcium carbonate formed is transferred to calciner for adsorbent regeneration (Chi, et al., 2017). In calciner, calcium carbonate broke down into calcium oxide and carbon dioxide at temperature between 650°C to 900°C, (He, et al., 2017). The CO_2 generated is compressed for storage and the regenerated calcium oxide is sent to carbonator for recycle (Chi, et al., 2017).

2.2 Recent Development on CaO-Based Adsorbent for CO_2 Capture

As mentioned, calcium oxide-based (CaO-based) adsorbent provides fast kinetics and relatively high theoretical CO_2 capture capacity of 0.786 g CO_2/ g CaO (Kazi, et al., 2014). However, it is susceptible to decrease in capture capacity after multiple high temperature carbonation and calcination cycles. The decrease in capture capacity is due to sintering and pore size reduction of adsorbent (Anthony, 2011). Besides the decreased capture capacity, the elevated carbonation temperature leads to high energy penalty. Recently, the problems mentioned had grabbed the researcher's attention to develop better adsorbents.

It is known that, addition of inert support to CaO-based adsorbent is able to improve its characteristics and performance. For instance, Kazi, et al. (2014) incorporated metal oxide stabilizer to improve the properties. Mayenite ($Ca_{12}Al_{14}O_{33}$) inert support was added to CaO by simple hydrothermal method. The adsorbent with composition of 27 wt% CaO and 73 wt% $Ca_{12}Al_{14}O_{33}$ under conditions of carbonation at 650 °C for 10 minutes as well as calcination at 920 °C for 3 minutes was studied. The adsorption capacity attained is 0.21 g CO_2/ g adsorbent, which is able to last for up to 40 cycles. The conversion achieved is almost equivalent to full conversion of the CaO available in the adsorbent. This achievement is contributed by the presence of water and support which aids the diffusion of CO_2 into CaO. Besides, inert support is able to overcome the thermal sintering problem of CaO particles, thus increasing the number of carbonation and calcination cycle. Apart from that, it is able to improve the mechanical stability, thus reducing the particle attrition and elutriation problem which makes it suitable to be used in fluidized bed. The synthesis method involved is more cost effective compared to Pechini method and the materials involved are easily obtainable at lower price compared to other type of metal oxides (Kazi, et al., 2014). Although this capture capacity obtained might seem attractive, it is considered low compared to the theoretical capture capacity mentioned in previous paragraph. According to the author, increasing the amount of CaO in $Ca_{12}Al_{14}O_{33}$ is able to increase the adsorption capacity, but the number of carbonation and calcination cycle will be sacrificed (Kazi, et al.,2014). In other words, although most of the problem mentioned can be solve, the adsorption capacity is sacrificed.

Similarly, Radfarnia and Sayari (2015) conducted studies between aluminium oxide support and CaO adsorbent. Instead of improving the inert support, the authors

concentrate on developing synthesis methods that give high dispersion of CaO adsorbent within the inert support structure. During research, the adsorbent was synthesised with citrate-assisted sol–gel technique and calcined in inert as well as air environment. The adsorbent with composition of 92.5 wt% CaO and 7.5 wt% $Ca_9Al_6O_8$ was tested under condition of carbonation 650 ℃ for 30 minutes and calcination of 800 ℃ for 10 minutes. It is able to achieve a high and stable adsorption capacity of 0.57 g CO_2/ g adsorbent for 31 carbonation-calcination cycles. This high stability is contributed by the presence of anhydrous citric acid which is able to modify the structure of CaO adsorbent. During calcination step, citric acid reacts with CaO to produce organic calcium salt under inert environment and combustion of the organic calcium salt in air environment form porous adsorbent by releasing certain amount of gases (Wang et al., 2013). In other words, CaO is chemically treated by citric acid to prevented agglomeration of CaO particles as well as to enhance the porosity and specific surface area of the adsorbent. Moreover, addition of citric acid aids the uniform distribution of CaO in $Ca_9Al_6O_8$ inert support which is able to reduce the thermal sintering problem. Although this method is able to give higher adsorption capacity, adsorbent attrition and high carbonation temperature is still a critical issue while pursuing to large-scale operation.

According to Wang et al. (2011), chemical treatment involved is simple and practical in large scale production, but the cost is still a concern. To solve this problem, Chi, et al. (2017) proposed by-product biodiesel (BPB) which is highly available in low price as an alternative solution. The author modified CaO adsorbent with BPB through combustion. The synthesised adsorbent with composition of 25 mL of BPB /g of CaO is tested under condition of carbonation at 700 ℃ for 20 minutes and calcination at 850 ºC for 10 minutes. After the chemical treatment, the adsorbent become more porous as well as has higher pore volume and surface area. Hence, giving a stable CO_2 capture capacity of 0.5 g CO_2/g adsorbent for up to 20 cycles. Besides, this combination provides superior sintering resistance which allows the adsorbent to maintain its adsorption capacity through more cycle.

Previously, most of the CaO-based adsorbent development are focussed on improving the adsorbent thermal stability and sintering resistance, which in turns increased the number of carbonation and calcination cycles at high carbonation temperature. However, lifetime of adsorbent is not the only issue that contribute to

high operating cost for CLP system. The elevated carbonation temperature issue which is less focussed on will contribute to high operating cost as well. Normally, the temperature of flue gas released from powerplant is between 100 to 150 °C (Mokhtar, Taib and Hassim, 2014). On the other hand, the temperature needed for CO_2 capture reaction in carbonation step is between 650 to 700°C. The differences between both temperatures is approximately 500 °C. Based on study, approximately 40 % additional energy consumption is required to raise the flue gas to desired temperature in order for the reaction to take place, thus leads to high energy penalty for high flow fossil fuel plant (Lee, et al., 2015). Hence, it is crucial to lower the carbonation temperature in order to minimize the energy consumption during CO_2 capture.

In order to avoid large energy penalty problem, Jing, et al. (2017) proposed to lower the carbonation temperature to 500 °C. Apart from energy saving, this may also ease the design of the reactor. The author studied the synthesised adsorbents under carbonation temperature of 500 °C for 30 min. Out of these adsorbents, the one with composition of 80 wt% CaO and 20 wt% of $Ca_3Al_2O_6$ is able to give the highest CO_2 capture capacity which is 0.19 g CO_2 / g adsorbent, which is five times higher than pure CO_2 adsorbent synthesised. Although addition of inert is able to decrease the diffusion resistance through product layer, this result is still not comparable with the theoretical CO_2 capture capacity mentioned previously.

Instead of adding inert, Lee, et al. (2015) added nickel oxide catalyst into the adsorbent. Currently, this method is believed to be the most promising pathway to prevent the thermal sintering and energy penalty problem. Instead of improving the stability of the adsorbent, the presence of catalyst is able to lower the carbonation temperature to 465°C. Out the adsorbents studied, the one with composition of 50 mol% CaO and 50 mol% NiO is able to give adsorption capacity of 0.68 g CO2/ g CaO, which is comparable with the theoretical CO_2 capture capacity mentioned previously. In other words, the root cause of thermal sintering and high energy penalty problem can be solved. However, the reaction kinetic is still unclear. Hence, the objective of this project is to study the kinetic of CaO-based adsorbent before and after addition of nickel oxide. A summary of various developments done recently to attempt to the problems mentioned is shown in Table 2.1.

Table 2.1: Comparison of Recent Development on CaO-Based Adsorbent for CO_2 Capture

Literature	Modified CaO-based adsorbent	Composition	Adsorption Capacity	Carbonation/ Calcination Cycle	Carbonation Temperature and Time	Advantages
Chi, et al. (2017)	By-product of biodiesel/ CaO	25 ml BPB/ g CaO	0.5 g CO_2/ g adsorbent	20	700 °C, 20 min	– greater sintering resistance – higher pore volume and surface area
Jing, et al. (2017)	CaO/ $Ca_3Al_2O_6$	80/ 20 wt %	0.19 g CO_2/ g adsorbent	60	500 °C, 30 min	– inert decreases the diffusion resistance of CO_2 through product layer – structure of inert contributed to thermal stable characteristic – reduced sintering effect – lower energy penalty
Kazi, et al. (2014)	CaO/ $Ca_{12}Al_{14}O_{33}$	27/ 73 wt%	0.21 g CO_2/ g adsorbent	40	650°C, 10 min	– structure of inert contributed to thermal stable characteristic – reduced sintering effect and improved stability of adsorbent – simpler and more cost-effective synthesis

Remark: N/A indicates the data is not available.

Table 2.1 (Continued)

Literature	Modified CaO-based adsorbent	Composition	Adsorption Capacity	Carbonation/ Calcination Cycle	Carbonation Temperature and Time	Advantages
Lee, et al. (2015)	CaO-NiO	50/ 50 mol%	0.68 g CO_2/ g CaO	N/A	465 °C, 30 min	– lower sorption temperature – lower energy consumption, energy penalty – simpler and more cost-effective synthesis
Radfarnia and Sayari (2015)	CaO/ $Ca_9Al_6O_{18}$	92.5/ 7.5 wt%	0.57 g CO_2/ g adsorbent	31	650 °C, N/A	– structure of inert contributed to thermal stable characteristic

Remark: N/A indicates the data is not available.

2.3 Kinetic Study

According to Tomaszewicz, Kotyczka-Morańska and Plis (2016), the efficiency of CO_2 capture depends on diffusion of CO_2. Since diffusion greatly relies on the kinetics of the reaction, it is crucial to understand it in order to enhance the performance of CaO-based adsorbent in CO_2 capture. The CO_2 capture reaction comprises of three different regimes. This includes a fast chemical reaction-controlled stage, followed by a slower transition stage and the slowest stage is controlled by the rate of CO_2 diffuse through the $CaCO_3$ layered formed to reach the fresh CaO (Kazi et al., 2014).

Over the years, there are various mathematical simulations developed based on the fundamental rate law model for kinetic modelling of solid-gas reaction like CO_2 capture. These models are developed based on the conversion of the solid which can be determined by measuring the mass change of solid with the aid of TGA. These models had been widely used in different applications. For instance, isothermal analysis was used to study CO_2 adsorption (Wei, et al., 2017), isoconversional analysis was used to study wood chips decomposition (Gašparovič, Koreňová and Jelemenský, 2010), Coats-Redfern (CR) method was used to study pyrolysis (Xiang, et al., 2018) as well as Kissenger–Akahira–Sunose (KAS) and Flynn–Wall–Ozawa (FWO) methods were used to study combustion of char (Islam, et al., 2016).

2.3.1 Isothermal Analysis Method

Isothermal analysis was applied to study the behaviour of activated carbon in CO_2 adsorption and desorption reaction (Wei, et al., 2017). The TGA test was conducted for three holding temperatures for period of 30 minutes for each reaction. After obtaining data from TGA, conversion, α of each reaction is calculated and computed into different $g(\alpha)$. Unique $g(\alpha)$ formula is assigned based on different kinetic mechanism as shown in Table 2.2.

Table 2.2: Kinetic Model for Each Stage (Wei, et al., 2017)

	Reaction Model	**Equation *g(α)***
Chemical Reaction-Controlled Stage	Zero-order (F_0)	α
	First-order (F_1)	$-\ln(1-\alpha)$
	Second-order (F_2)	$(1-\alpha)^{-1}-1$
	Third-order (F_3)	$[(1-\alpha)^{-2}-1]/2$
Diffusion-Controlled Stage	One-dimensional diffusion (D_1)	α^2
	Two-dimensional diffusion (D_2)	$(1-\alpha)\ln(1-\alpha)+\alpha$
	Three-dimensional diffusion Jander Equation (D_3)	$[1-(1-\alpha)^{1/3}]^2$
	Three-dimensional diffusion Ginstling-Brounshtein (D_4)	$\left(1-\frac{2\alpha}{3}\right)-(1-\alpha)^{2/3}$

Each unique *g(α)* varies with time is plotted as shown in the Eq. 2.1 to select the most probable *g(α)* to describe each mechanism. Two assumptions of this equation are isobaric condition and mass transfer limitation is negligible.

$$g(\alpha) = k(T)t \qquad \text{(Eq. 2.1)}$$

where

g(α) = integral form of the reaction model

α = conversion of adsorbent

k(T) = function of rate constant, min^{-1}

t = time, min

The *g(α)* should give linear relationship with time, thus the model that give maximum linear correlation will be chosen as the most suitable mechanism to describe the reaction. In other words, linear model that give r-squared, R^2 value nearest to 1 is selected. Based on the selected mechanism, the rate limiting factor of each reaction is known and researcher can focus on improving it in order to develop

better adsorbent. Upon selecting the best model, the gradient of *g(α)* against time is collected for each temperature as rate constant, k. Next, the *ln(k)* is plotted against $-\frac{1}{T}$ to give Arrhenius equation as shown in Eq. 2.2.

$$\ln k(T) = \ln A - \frac{E}{RT} \qquad \text{(Eq. 2.2)}$$

where

k(T) = function of rate constant, min^{-1}

A = pre-exponential factor, min^{-1}

E = activation energy, J mol^{-1}

R = universal ideal gas constant = 8.314 J mol^{-1} K^{-1}

T = temperature, K

Based on Arrhenius equation, activation energy, *E* and pre-exponential factor, *A* can be calculated from the gradient and y-intercept respectively.

2.3.2 Isoconversional Method

Since there is not much literature review of kinetic study from the field of CO_2 capture can be learnt from, other kinetic modelling of solid-gas reaction can be served as reference as well. For instance, isoconversional method was applied to study the decomposition kinetics of wood chip with the aid of TGA (Gašparovič, Koreňová and Jelemenský, 2010). This model involves study of sample mass loss at four different heating rates. The four heating rates was used to calculate the actual temperature based on Eq. 2.3

$$T = T_o + \beta t \qquad \text{(Eq. 2.3)}$$

where

T = actual temperature, K

T_0 = initial temperature, K

β = heating rate, K/min

t = time, min

Upon obtaining the mass loss data from TGA, conversion data was calculated to plot $\ln\left(\frac{d\alpha}{dt}\right)_\alpha$ against $-\frac{1}{T_\alpha}$ as shown in Eq. 2.4. This is a linear model, thus the reaction order, *n* that give r-squared, R^2 nearest to 1 justifies the suitability of the reaction data on this model.

$$\ln\left(\frac{d\alpha}{dt}\right)_\alpha = \mathrm{n}\ln(1-\alpha) + \ln A_\alpha - \frac{E_\alpha}{RT_\alpha} \qquad \text{(Eq. 2.4)}$$

where

α = conversion of adsorbent

t = time, min

$\left(\frac{d\alpha}{dt}\right)_\alpha$ = degree of conversion, min^{-1}

n = reaction order

A_α = apparent pre-exponential factor, min^{-1}

E_α = apparent activation energy, J mol^{-1}

R = universal ideal gas constant = 8.314 J mol^{-1} K^{-1}

T_α = temperature, K

Based on Eq. 2.4, kinetic parameters including apparent pre-exponential factor, A_α and apparent activation energy, E_α can be obtained from the y-intercept and gradient respectively. However, the kinetic parameters obtained are not for the whole decomposition process and varies across different conversion. Hence, causing the data complicated to be compared with another sample. In addition, isoconversional method is used for complex processes study which involves multiple chemical reactions running simultaneously. Hence, unlike isothermal analysis it is unable to determine the specific mechanism involved in the reaction.

2.3.3 Coats-Redfern (CR) Method

Coats-Redfern (CR) method is used to study kinetic of solid-gas reaction. It was applied to study pyrolysis of biomass (Xiang, et al., 2018). With the aid of this model, the catalytic and non-catalytic reaction mechanism of each sample can be identified. Conversion data of different heating rate was obtained from TGA to calculate each *g(α)* as shown in Table 2.2. Next, $\ln\frac{g(\alpha)}{T^2}$ is plot against $-\frac{1}{T}$ as shown in Eq. 2.5 The *g(α)* that give r-squared, R^2 nearest to 1 prove the reaction data best fit the model.

$$\ln\frac{g(\alpha)}{T^2} = \ln\frac{AR}{\beta E} - \frac{E}{RT} \qquad \text{(Eq. 2.5)}$$

where

α = conversion of adsorbent

n = reaction order

T = temperature, K

A = pre-exponential factor, min^{-1}

R = universal ideal gas constant = 8.314 J mol^{-1} K^{-1}

β = heating rate, K/min

E = activation energy, J mol^{-1}

Based on this relationship, activation energy, E and pre-exponential factor, A can be calculated from the gradient and intercept.

2.3.4 Kissenger–Akahira–Sunose (KAS) Method

KAS method was applied to study the kinetic of solid-gas reaction, combustion of char (Islam, et al., 2016). Mass change data was obtained for three different heating rates with the aid of TGA and converted into conversion data. Conversion data obtained was converted into each *g(α)* as shown in Table 2.2. Next, $\ln\frac{\beta}{T^2}$ is plot against $-\frac{1}{T}$ as shown in Eq. 2.6. The *g(α)* that give r-squared, R^2 nearest to 1 prove the reaction data best fit the model.

$$\ln\frac{\beta}{T^2} = \ln\frac{AE}{Rg(\alpha)} - \frac{E}{RT} \qquad \text{(Eq. 2.6)}$$

where

β = heating rate, K/min

T = temperature, K

A = pre-exponential factor, min^{-1}

E = activation energy, J mol^{-1}

R = universal ideal gas constant = 8.314 J mol^{-1} K^{-1}

$g(\alpha)$ = integral function of conversion

α = conversion of adsorbent

Based on this relationship, activation energy, *E* and pre-exponential factor, *A* can be calculated from the gradient and intercept.

2.3.5 Flynn–Wall–Ozawa (FWO) Method

Flynn–Wall–Ozawa (FWO) methods were used to study combustion of char (Islam, et al., 2016). This method was derived from Doyle's approximation. Mass change data was obtained for three different heating rates with the aid of TGA and converted into conversion data. Conversion data obtained was converted into each $g(\alpha)$ as shown in Table 2.2. Next,$\ln\beta$ is plot against $-\frac{1}{T}$ as shown in Eq. 2.7. The $g(\alpha)$ that give r-squared, R^2 nearest to 1 prove the reaction data best fit the model.

$$\ln\beta = \ln\frac{AE}{Rg(\alpha)} - 5.331 - 1.052\frac{E}{RT} \qquad \text{(Eq. 2.7)}$$

where

β = heating rate, K/min

A = pre-exponential factor, min^{-1}

E = activation energy, J mol^{-1}

R = universal ideal gas constant = 8.314 J mol^{-1} K^{-1}

$g(\alpha)$ = integral function of conversion

T = temperature, K

α = conversion of adsorbent

Based on this relationship, activation energy, *E* and pre-exponential factor, *A* can be calculated from the gradient and intercept.

2.3.6 Kinetic Model Selection

In short, there are various mathematical models developed based on the fundamental rate law model for kinetic modelling of solid-gas reaction as summarised in Table 2.3. Each model has its pros and cons in different applications. Firstly, all the kinetic model mentioned do not need any previous understanding on the reaction mechanism (Islam, et al., 2016). Besides, all the models are able to give both kinetic parameters including activation energy, *E* and pre-exponential factor, *A*. Moreover, the order of reaction can be obtained as well.

Isothermal analysis is most suitable to study the kinetic of CaO-based adosbent for CO_2 capture. It is simple and more reliable compared to non-isothermal analysis. Isothermal model is dependent to time, while non-isothermal model is dependent on heating rate. It is known that heating rate is easily affected by the sample size and shape (Diefallah et al., 1987). Besides, for non-isothermal analysis, activation energy obtained is in a range instead of single value (Gašparovič, Koreňová and Jelemenský, 2010). Hence, this may make the comparison of performance of each sample harder.

Isoconversional, CR, KAS and FWO models are not suitable for this study. Instead of studying the kinetic of adsorption around 450 °C, these models provide study over a wide range of temperature under constant heating rate. Hence, Isothermal analysis might be a better candidate to model the kinetic of this study. By holding few constant temperatures data around 450 °C, change in adsorbent mass against time can be obtain can fit into this model.

Table 2.3: Comparison of Thermal Analysis Model

Model	**Isothermal Analysis**	**Isoconversional**	**Coats-Redfern (CR)**	**Kissenger–Akahira–Sunose (KAS)**	**Flynn–Wall–Ozawa (FWO)**
Literature	Wei, et al. (2017)	Gašparovič, Koreňová and Jelemenský (2010)	Xiang, et al. (2018)	Islam, et al. (2016)	Islam, et al. (2016)
TGA Condition	Isothermal	Non-isothermal	Non-isothermal	Non-isothermal	Non-isothermal
Similar Characteristics	– Describe reaction without information of reaction mechanism – Can give both kinetic parameters *A* and *E* from TGA data – Apparent reaction order, *n* can be obtained				
Distinct Characteristic	– Simple Model – Independent of heating rate, β – Conversion of adsorbent, α depends on time	– Simple Model – Dependent of heating rate, β – rate of reaction depends on temperature	– Relatively complicated model – dependent on heating rate, β – Conversion of adsorbent, α depends on temperature	– Relatively complicated model – dependent on heating rate, β	– Relatively complicated model – dependent on heating rate, β

Table 2.3 (Continued)

Model	Isothermal Analysis	Isoconversional	Coats-Redfern (CR)	Kissenger–Akahira–Sunose (KAS)	Flynn–Wall–Ozawa (FWO)
Simplified Model	$g(\alpha) = k(T)t$ (Eq. 2.1)	$\ln\frac{d\alpha}{dt} = \mathrm{n}\ln(1-\alpha) + \ln A - \frac{E}{RT}$ (Eq. 2.4)	$\ln\frac{g(\alpha)}{T^2} = \ln\frac{AR}{\beta E} - \frac{E}{RT}$ (Eq. 2.5) where $T = T_0 + \beta \mathrm{t}$	$\ln\frac{\beta}{T^2} = \ln\frac{AE}{Rg(\alpha)} - \frac{E}{RT}$ (Eq. 2.6) where $T = T_0 + \beta \mathrm{t}$	$\ln\beta = \ln\frac{AE}{Rg(\alpha)} - 5.331 - 1.052\frac{E}{RT}$ (Eq. 2.7) where $T = T_0 + \beta \mathrm{t}$
Plot	$g(\alpha)$ against t	$\ln\frac{d\alpha}{dt}$ against $-\frac{1}{T}$	$\ln\frac{g(\alpha)}{T^2}$ against $-\frac{1}{T}$	$\ln\frac{\beta}{T^2}$ against $-\frac{1}{T}$	$\ln\beta$ against $-\frac{1}{T}$
Slope	$\ln k(T) = \ln A - \frac{E}{RT}$ (Eq. 2.2)	$\frac{E}{R}$	$\frac{E}{R}$	$\frac{E}{R}$	$\frac{E}{R}$
Y-intercept	0	$n\,ln(1-\alpha) + ln\,A$	$ln\frac{AR}{\beta E}$	$ln\frac{AE}{Rg(\alpha)}$	$ln\frac{AE}{Rg(\alpha)} - 5.331$

CHAPTER 3

METHODOLOGY AND WORK PLAN

3.1 Materials and Apparatus

There are several materials and apparatus needed to complete this research. All the material and apparatus listed below were prepared before the studies were carried out.

3.1.1 Materials and Chemicals

The raw materials and chemicals needed for this research are presented in Table 3.1.

Table 3.1: List of Raw Material and Chemical Used

Chemicals	Quantity	Brand	Purpose
Calcium nitrate tetrahydrate $Ca(NO_3)_2 \cdot 4H_2O$	11 g	Merck	Metal precursor for adsorbent synthesis
Nickel (II) nitrate hexahydrate $Ni(NO_3)_2 \cdot 6H_2O$	7 g	Merck	Metal precursor for adsorbent synthesis
Citric acid $C_6H_8O_7$	40 g	Merck	Binder for adsorbent synthesis
Distilled Water H_2O	-	UTAR	To dissolve metal precursor mixture

3.1.2 Apparatus and Equipment

The apparatus and equipment needed for this study are tabulated in Table 3.2 whilst the instruments needed are shown in Table 3.3.

Table 3.2: List of Apparatus and Equipment Used

Apparatus and Equipment	Specification	Purpose
Oven	Memmert, 100 °C	To dry the sample gel
Programmable Furnace	Wise Therm FP-03, 700 °C	To calcine the sample gel
Hot Plate Stirrer	IKA RH basic 2	To stir and heat up solution during sample synthesis

Table 3.3: List of Instruments Used

Instrument	Specification	Purpose
Thermogravimetric Analyser (TGA)	Perkin Elmer STA 8000	To perform CO_2 adsorption study
X-ray Diffractometer (XRD)	Shimadzu XRD-6000	To determine the crystalline structure of adsorbent
Scanning Electron Microscope - Energy Dispersive X-ray Analyzer (SEM-EDX)	Hitachi Model S-3400N	To obtain surface morphology and composition of adsorbent

3.2 Research Flow Diagram

Research flow diagram depicts the overall research plan involved in this project. It constitutes of several experimental steps with kinetic study as the main focus of this project. The summary of research methodology and study direction is shown in Figure 3.1.

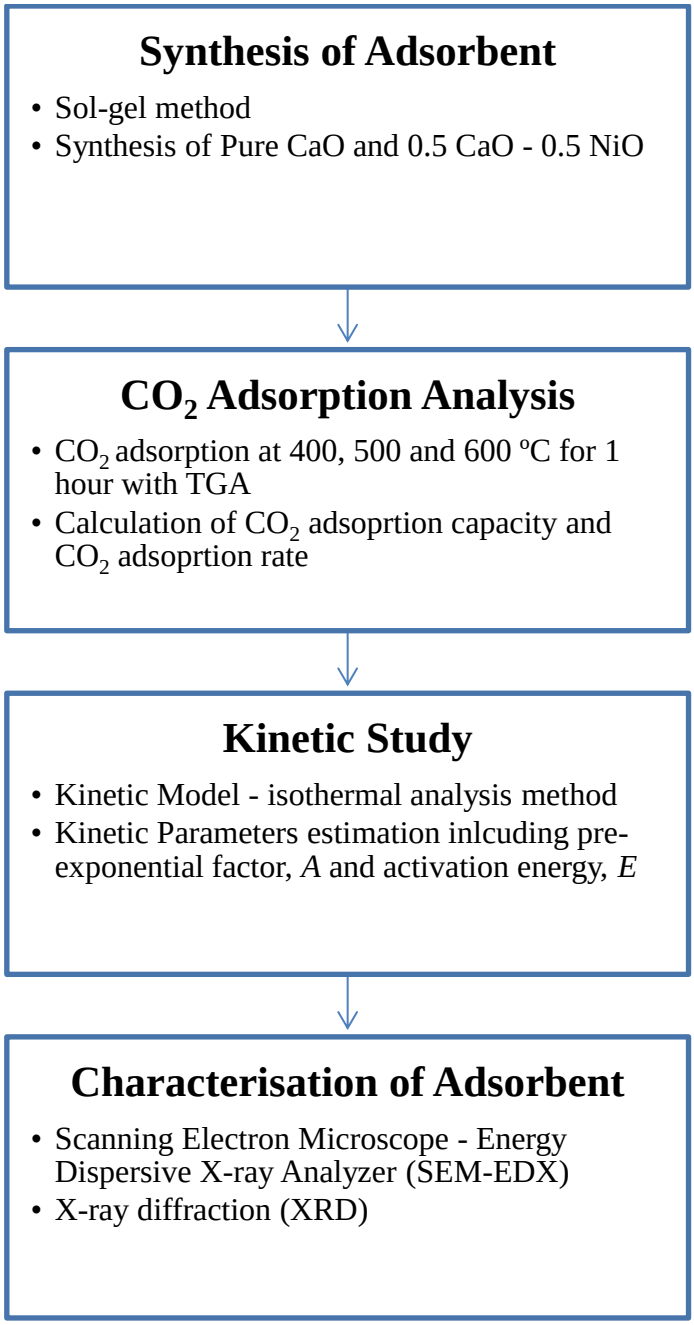

Figure 3.1: Research Flow Diagram

3.3 Synthesis of Adsorbent

Sol-gel method was applied to synthesise the adsorbents needed in this project. To synthesise 0.5 CaO- 0.5 NiO adsorbent, calcium nitrate tetrahydrate and nickel (II) nitrate hexahydrate were mixed with molar ratio of 0.5: 0.5. After preparing the precursors mixture, citric acid was added with the molar ratio of precursor mixture to citric acid of 1: 3. Next, water was added to dissolve the mixture with molar ratio of mixture to water of 1: 125. The mixture produced was heated at 90 °C under vigorous stirring until the gel was formed with the aid of hot plate magnetic stirrer. The gel formed was allowed to dry in an oven at 100 °C for 1 hour. The dried gel was calcined in furnace at 700 °C for 4 hours. The steps above were repeated by replacing the metal precursors mixture with pure calcium nitrate tetrahydrate to synthesis pure CaO.

3.4 CO_2 Adsorption Analysis

The ability of CO_2 adsorption for both adsorbents at 400, 500 and 600 °C were tested with the aid of TGA. Before running the test, the sample was heated to 700 °C at rate of 20 °C/min to conduct pre-treatment. During pre-treatment 20 ml/min nitrogen gas was flown through the samples at holding temperature of 700 °C for 10 min. After pre-treatment, the sample temperature was allowed to drop to the desired temperatures of 400 °C, 500 °C and 600 °C respectively at a rate of 20 °C/min. Upon achieving the desired temperature, 20 ml/min of CO_2 was allowed to flow through the sample for 60 minutes. The mass change involved was recorded by TGA and CO_2 adsorption rates can be computed as shown in Eq. 3.1 with the unit of mg CO_2/ mg CaO. Since NiO catalyst will be added into the adsorbent, the mass fraction of CaO in the adsorbent need to be considered.

$$CO_2\ adsorption\ rate\ = \frac{m(t) - m(0)}{m(0) \times f_{CaO} \times t} \qquad \text{(Eq. 3.1)}$$

where

m(0) = mass of adsorbent at time 0, mg

m(t) = mass of adsorbent at time t, mg

f_{CaO} = mass fraction of CaO in adsorbent

t = time, min

The adsorption capacity which is also known as the conversion of CaO adsorbent can be defined as amount of CO_2 captured by the CaO available. It can be obtained by the formula provided in Eq. 3.2 and expressed in mg CO_2/ mg CaO.

$$CO_2\ adsorption\ capacity\ = \alpha\ = \frac{m(t) - m(0)}{m(0) \times f_{CaO}} \qquad \text{(Eq. 3.2)}$$

where

α = conversion

$m(0)$ = mass of adsorbent at time 0, mg

$m(t)$ = mass of adsorbent at time t, mg

f_{CaO} = mass fraction of CaO in adsorbent

3.5 Kinetic Study

The kinetic study on CaO-based adsorbent for CO_2 capture can be scrutinised by means of developed mathematical kinetic models. The kinetic model applied was the isothermal analysis method represented in Eq. 3.3 (Wei, et al., 2017).

$$g(\alpha) = k(T)t \qquad \text{(Eq. 3.3)}$$

where

$g(\alpha)$ = integral form of the reaction model

$k(T)$ = function of rate constant, min^{-1}

t = time, min

Eq. 3.3 is a linear regression equation which involves $g(\alpha)$ against t. The reaction involved can be divided into three parts including chemical reaction-controlled, transition and diffusion-controlled reaction. Chemical reaction-controlled reaction has the highest rate of reaction, followed by transition stage which is slower and diffusion-controlled which is the slowest. It is noted that transition stage was controlled more by diffusion limitation than chemical reaction limitation, thus diffusion-controlled model was used for transition stage. Hence, in order to acquire the most probable mechanism function different model as shown in Table 3.4 is applied by plotting $g(\alpha)$ against t. The gradient of the plot is function of rate constant, $k(T)$, whereby k_c denotes the rate constant for chemical reaction-controlled stage, k_t denotes rate constant for transition stage and k_d denotes the rate constant for

diffusion-controlled stage. Meanwhile, regression analysis was carried out to determine the suitability of each models. In other words, data with R-squared, R^2 nearest to 1 suits the model best.

Table 3.4: Kinetic Model for Each Stage (Wei, et al., 2017)

	Reaction Model	**Equation *g(α)***
Chemical Reaction-Controlled Stage	Zero-order (F_0)	α
	First-order (F_1)	$-\ln(1-\alpha)$
	Second-order (F_2)	$(1-\alpha)^{-1}-1$
	Third-order (F_3)	$[(1-\alpha)^{-2}-1]/2$
Diffusion-Controlled Stage	One-dimensional diffusion (D_1)	α^2
	Two-dimensional diffusion (D_2)	$(1-\alpha)\ln(1-\alpha)+\alpha$
	Three-dimensional diffusion Jander Equation (D_3)	$[1-(1-\alpha)^{1/3}]^2$
	Three-dimensional diffusion Ginstling-Brounshtein (D_4)	$\left(1-\frac{2\alpha}{3}\right)-(1-\alpha)^{2/3}$

Next, rate constant, *k(T)* obtained for 400, 500 and 600 ºC for each model were plotted against -1/Temperature to obtain Arrhenius plot. From this plot, pre-exponential factor, A and activation energy, E can be calculated with Eq. 3.4. Apart from that, regression analysis was carried out to determine the suitability of the data to the Arrhenius equation.

$$\ln k(T) = \ln A - \frac{E}{RT} \qquad \text{(Eq. 3.4)}$$

where

A = pre-exponential factor, s^{-1}

E = activation energy, J mol^{-1}

R = gas constant = 8.314 J mol^{-1} K^{-1}

T = reaction temperature, K

3.6 Characterisation of Adsorbent

Characterisation was carried out to study the effect of nickel oxide catalyst on the chemical and physical properties of the adsorbent. By understanding the nature of each adsorbent, the catalytic performance can be explained. The instruments used were Scanning Electron Microscope - Energy Dispersive X-ray Analyzer (SEM-EDX) as well as X-ray diffraction (XRD).

3.6.1 Scanning Electron Microscope - Energy Dispersive X-ray Analyzer (SEM-EDX)

SEM Hitachi Model S-3400N was used to study the changes of surface and structure morphology. Before analysing, the samples were enveloped with a thin layer of gold by using Emitech SC7620 Sputter Coater. The adsorbents were scanned at the magnification of x5.5k with voltage of 15 kV. High resolution images of morphology and crystallographic structure of adsorbent were generated to aid the studies of adsorbent. Besides, Energy Dispersive X-ray Analyzer (EDX) connected to SEM was used to identify the weight percentage of different element presented in the adsorbent. The distribution of different elements inside the adsorbent was obtained by testing the weight percentage at four different spots on the sample.

3.6.2 X-ray diffraction (XRD)

XRD is a non-destructive technique dedicated for characterisation of crystalline materials. In this study, it was used to identify the components present in the adsorbents. Shimadzu XRD-6000 was used to conduct the test at room temperature and CuKα radiation operated at 40 kV and 30 mA. The X-ray diffractogram was collected in the range of 2θ = 20° - 80° with sweep rate of 2 °/min. Besides, average crystallite size can be computed from the 3 strongest peaks obtained with the aid of Debye-Scherrer's equation displayed in Eq. 3.5 (Guire et al., 2004).

$$d_x = \frac{0.94\lambda}{FWHM.cos\theta} \qquad \text{(Eq. 3.5)}$$

where

d_x = Crystallite size, nm

λ = wavelength of X−ray = 0.15406nm (CuKα)

$FWHM$ = Full Width at Half Maximum, rad

θ = Bragg angle, rad

CHAPTER 4

RESULTS AND DISCUSSION

4.1 CO_2 Adsorption Analysis

To study the effect of carbonation temperature on the performance of the synthesised calcium oxide (CaO) and calcium oxide-nickel oxide (CaO-NiO) adsorbents, carbonation was conducted by thermogravimetric analyser (TGA) at temperature of 400, 500 and 600 ºC. The mass increase over time profile obtained from TGA represents the amount of carbon dioxide (CO_2) captured reacted during the process of carbonation of CaO-based adsorbent and turned into calcium carbonate ($CaCO_3$) over time. The raw data obtained from TGA is shown in appendix A. The data obtained was computed into adsorption capacity curve as shown in Figures 4.1 and 4.2.

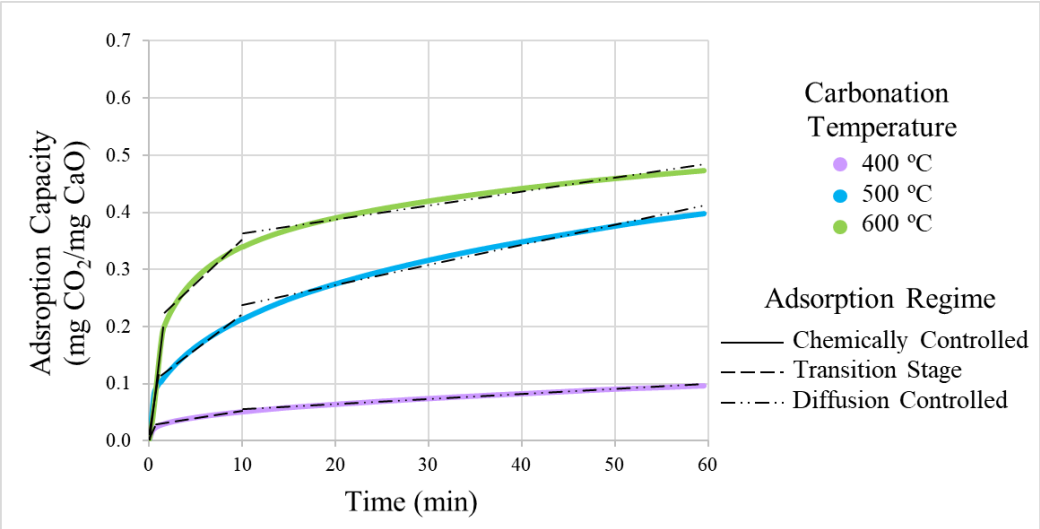

Figure 4.1: Adsorption Capacity Curve for Calcium Oxide (CaO) Adsorbent at Carbonation Temperature of 400, 500 and 600 °C

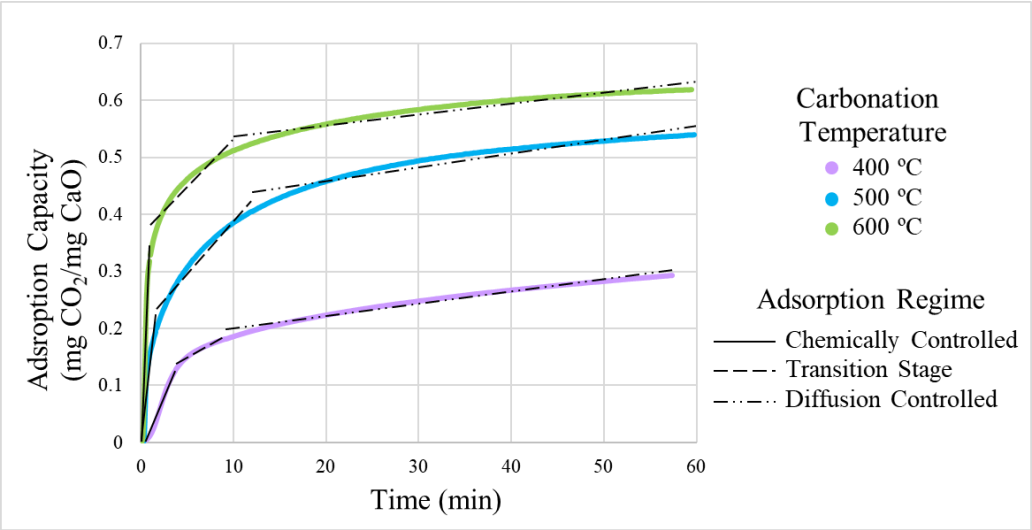

Figure 4.2: Adsorption Capacity for Calcium Oxide-Nickel Oxide (CaO-NiO) Adsorbent at Carbonation Temperature of 400, 500 and 600 °C

4.1.1 Adsorption Regime

By observing the adsorption capacity curve, it is shown that the CO_2 adsorption rate increased rapidly in the first few minutes and slow down to reach plateau. This clearly indicated that the CO_2 capture profile comprised of three different regimes. The rapid increase in CO_2 adsorption rate at the beginning shows that the carbonation reaction rate was controlled by chemical reaction. Next, the decrease in adsorption rate shows a transition from chemical reaction-controlled stage into diffusion-controlled stage. The profile ended with a plateau indicates the diffusion-controlled reaction (Tomaszewicz, Kotyczka-Morańska and Plis, 2016).

During the chemical reaction-controlled stage, reaction occurs on free surface of CaO-based adsorbents. The rate of reaction involved is restricted by the kinetic reaction between the adsorbent and CO_2. During transition stage, formation of solid product produces a layer of $CaCO_3$ enveloping the active surface of CaO particles, thus increasing the impact on surface reaction. In diffusion-controlled stage, the reaction between the adsorbent and CO_2 is physically restricted by the increasing steric hindrance for CO_2 to diffuse through the carbonated layer and contact with the unreacted CaO core. Thus, resulting to a slower carbonation rate (Nimmas et al., 2018).

4.1.2 Adsorption Rates

By analysing the TGA profile, the CO_2 adsorption rate for CaO and CaO-NiO were displayed in Table 4.1. The sample calculation for adsorption rate is shown in appendix B. The adsorption rate indicates the speed of CO_2 captured and reacted to form $CaCO_3$ at each stage based on the amount of CaO adsorbent supplied. It is noticed that the adsorption rate increases with increasing temperature. The elevation of temperature increases the average kinetic energy of reactants, thus enabling more reactants to have enough energy for effective collision to occur. By having more effective collision means more reactants are oriented correctly to ease the bond breaking and formation as well as rearrangement of atom to form $CaCO_3$ (Anthony, 2011). This phenomenon in turns increases the adsorption rate at higher carbonation temperature.

Table 4.1: Adsorption Rate of CaO and CaO-NiO Adsorbents

Type of Adsorbent	**Carbonation Temperature**	**Adsorption Rate (mg CO_2/ mg CaO. min)**		
		Chemically Controlled	**Transition Stage**	**Diffusion Controlled**
CaO	**400 ºC**	0.0330	0.0029	0.0009
	500 ºC	0.0909	0.0115	0.0031
	600 ºC	0.1298	0.0139	0.0020
CaO-NiO	**400 ºC**	0.0341	0.0097	0.0021
	500 ºC	0.1214	0.0185	0.0024
	600 ºC	0.3533	0.0262	0.0018

Based on the results for both adsorbents, chemically controlled stage had the highest adsorption rate as the reaction is occurred on the free surface of CaO. In transition stage, the adsorption rate dropped significantly as the formation of $CaCO_3$ layer obstruct the route for CO_2 to contact with unreacted CaO. Finally, diffusion-controlled stage gives the lowest adsorption rate as the $CaCO_3$ layer grows thicker with time. This justifies the observation made in previous part.

Besides, addition of NiO catalyst is able to speed up the CO_2 adsorption rate in chemically-controlled stage and transition stage. The potential of nickel transition

metal to form oxides with distinct valence states makes NiO a suitable catalyst for CO_2 capture. It is known that, Ni_2O_3 decompose to form NiO at 450 ºC. The excess oxygen detached from the NiO catalyst to offer oxygen vacancies for CO_2 capture to take place (Lee et al., 2015). Hence, with the presence of more oxygen vacancies, it is easier for CO_2 to attach to CaO, thus increasing the adsorption rate.

4.1.3 Adsorption Capacities

By analysing the TGA profile, the CO_2 adsorption capacity for CaO and CaO-NiO were shown in Table 4.2. The sample calculation for adsorption capacity is shown in appendix B. The adsorption capacity demonstrates the amount of CO_2 captured and reacted to form $CaCO_3$ at each stage per amount of CaO adsorbent supplied. Based on the results for CaO adsorbent carbonated at 600 ºC and CaO-NiO adsorbents at all carbonation temperatures, CO_2 adsorption favours chemically-controlled stage as it gives the highest adsorption capacity out of the three stages and it accounts half of the total adsorption capacity. As discussed previously, this is due to no impedance exists in the beginning, more CO_2 can reach the CaO active site and perform reaction easily without obstruction.

Table 4.2: Adsorption Capacity of CaO and CaO-NiO Adsorbents

Type of Adsorbent	**Carbonation Temperature**	**Adsorption Rate (mg CO_2/ mg CaO. min)**			
		Chemically Controlled	**Transition Stage**	**Diffusion Controlled**	**Total**
CaO	**400 ºC**	0.0231	0.0265	0.0433	**0.0929**
	500 ºC	0.1000	0.0999	0.1524	**0.3523**
	600 ºC	0.1947	0.1165	0.0991	**0.4104**
CaO-NiO	**400 ºC**	0.1260	0.0503	0.1037	**0.2800**
	500 ºC	0.1943	0.1889	0.1148	**0.4980**
	600 ºC	0.3180	0.1596	0.0875	**0.5651**

However, for CaO adsorbent carbonated at 400 and 500 ºC, adsorption capacity is highest at diffusion-controlled stage which accounts almost half of the total adsorption capacity. This is due to the reaction consists of shorter chemically-

controlled stage and transition stage, which contributes to low adsorption capacity in the first two stages. This is probably due to lower carbonation temperature providing insufficient energy for effective collision to occur, causing most of the reaction to happen outside the pores and blocked the pores. Hence, causing the reaction to enter diffusion-controlled stage earlier.

Besides, it is noted that the highest adsorption capacity achieved is 0.5661 mg CO_2/ mg CaO (56.61 %) which is still far from 100 % conversion. This is due to the reaction time is insufficient for adsorbent to completely react with CO_2. It can be observed from Figure 4.1, only CaO adsorbent with carbonation temperature of 400 ºC had reach plateau at the end of the curve. The rest of the adsorption capacity curve are still far from reaching plateau. Hence, there are still room for improvement for adsorption capacity if the carbonation time is extended.

Besides, addition of NiO catalyst into CaO adsorbent shows significant improvement of capture capacity. For instance, the adsorption capacity at 400 ºC increased from 0.0929 mg CO_2/ mg CaO to 0.2800 mg CO_2/ mg CaO after addition of NiO catalyst. Mixture of CaO and NiO increases the porosity of the adsorbent, contributing to more capacity for CaO to bond with CO_2. Thus, allowing the adsorption capacity of CaO-NiO adsorbent to improve significantly compared to CaO adsorbent at same carbonation temperature.

As mentioned previously, elevated carbonation temperature will contribute to high operating cost in CLP. Hence, it is crucial to lower the carbonation temperature in order to minimize the energy consumption during CO_2 capture. Since the adsorption capacity after addition of NiO catalyst still shows increasing trend with higher temperature, it is hard to conclude whether it will continue increase or remain constant after 600 ºC. Hence, the elevation temperature problem mentioned is still remain unanswered. However, it is confirmed that the addition of NiO catalyst is able to improve the performance of CaO adsorbent.

4.2 Kinetic Study

Kinetic analysis of CaO-based adsorbent in carbonation reaction had been conducted with the aid of adsorption capacity curve obtained. As mentioned, there are three different reaction regimes involved in CO_2 capture. Different type of isothermal kinetic models was applied on each regime to determine the most probable mechanism function. For instance, zero-order (F_0), first-order (F_1), second-order (F_2) and third-order (F_3) reaction model was applied in chemicall-controlled stage. One-dimensional diffusion (D_1), two-dimensional diffusion (D_2), three-dimensional diffusion Jander Equation (D_3) and three-dimensional diffusion Ginstling-Brounshtein (D_4) was applied in transition stage and diffusion-controlled stage.

4.2.1 Kinetic Study for Calcium Oxide Adsorbent

After conducting model fitting for CaO, the results obtained for chemical controlled stage is tabulated in Table 4.3, for transition stage is tabulated in Table 4.4 and for diffusion-controlled stage is tabulated in Table 4.5.

Table 4.3: Model fitting of CaO Adsorbent for Chemical Controlled Stage

Reaction Model	**Carbonation Temperature, *T***	**Rate Constant, k_c (min^{-1})**	**R^2 for *g(α)* vs *t***	**Activation Energy, *E* (J/mol)**	**Pre-exponential factor, *A* (min^{-1})**	**R^2 for *ln(k)* vs *-1/T***
F_0	400 ºC	0.0348	0.9534	34511.41	17.7787	0.9644
	500 ºC	0.0968	0.9157			
	600 ºC	0.1401	0.9952			
F_1	400 ºC	0.0352	0.9543	36752.04	26.7999	0.9698
	500 ºC	0.1026	0.9205			
	600 ºC	0.1554	0.9928			
F_2	400 ºC	0.0357	0.9553	38995.99	40.4878	0.9750
	500 ºC	0.1087	0.9250			
	600 ºC	0.1729	0.9890			
F_3	**400 ºC**	**0.0361**	**0.9562**	**41381.27**	**62.5646**	**0.9792**
	500 ºC	**0.1153**	**0.9292**			
	600 ºC	**0.1929**	**0.9837**			

Table 4.4: Model fitting of CaO Adsorbent for Transition Stage

Reaction Model	**Carbonation Temperature, *T***	**Rate Constant, k_t (min^{-1})**	**R^2 for *g(α)* vs *t***	**Activation Energy, *E* (J/mol)**	**Pre-exponential factor, *A* (min^{-1})**	**R^2 for *ln(k)* vs *-1/T***
D_1	400 ºC	0.0002	0.9923	93690.47	4810.2291	0.9362
	500 ºC	0.0040	0.9981			
	600 ºC	0.0086	0.9792			
D_2	400 ºC	0.0001	0.9926	97855.78	5061.4081	0.9414
	500 ºC	0.0022	0.9987			
	600 ºC	0.0051	0.9824			
D_3	**400 ºC**	**0.0000**	**0.9929**	**103758.72**	**2900.6786**	**0.9485**
	500 ºC	**0.0005**	**0.9993**			
	600 ºC	**0.0013**	**0.9855**			
D_4	400 ºC	0.0000	0.9927	101896.38	2107.5892	0.9414
	500 ºC	0.0005	0.9989			
	600 ºC	0.0012	0.9835			

Table 4.5: Model fitting of CaO Adsorbent for Diffusion Controlled Stage

Reaction Model	**Carbonation Temperature, *T***	**Rate Constant, k_d (min^{-1})**	**R^2 for *g(α)* vs *t***	**Activation Energy, *E* (J/mol)**	**Pre-exponential factor, *A* (min^{-1})**	**R^2 for *ln(k)* vs *-1/T***
D_1	400 ºC	0.0001	0.9991	76098.04	120.7594	0.7899
	500 ºC	0.0022	0.9937			
	600 ºC	0.0020	0.9750			
D_2	400 ºC	0.0001	0.9993	74020.37	56.2103	0.8116
	500 ºC	0.0013	0.9960			
	600 ºC	0.0013	0.9789			
D_3	**400 ºC**	**0.0000**	**0.9994**	**75898.51**	**22.6736**	**0.8116**
	500 ºC	**0.0004**	**0.9978**			
	600 ºC	**0.0004**	**0.9829**			
D_4	400 ºC	0.0000	0.9993	68609.62	5.9441	0.8116
	500 ºC	0.0003	0.9967			
	600 ºC	0.0003	0.9803			

Based on results obtained from regression analysis, the model that give highest R^2 value for both *g(α)* vs *t* and *ln(k)* vs *1/T* relationships is most suitable to describe the kinetic behaviour of the adsorbent. At chemical-controlled stage, third-order reaction model (F_3) best describes the kinetic behaviour of CaO adsorbent. At transition stage and diffusion-controlled stage, three-dimensional diffusion Jander Equation (D_3) is the best model to describe the behaviour of CaO adsorbent, which the reaction involved diffusion-controlled reaction in a sphere (Diefallah et al., 1987). The models verify the statement in previous part whereby there exists three different reaction regimes during CO_2 capture.

Figure 4.3, Figure 4.4, Figure 4.5 shows the plot of *g(α)* vs *t* for the best fit model at each stage for carbonation temperature of 400, 500 and 600 ºC respectively. In these figures, the y-axis on the left is for chemical controlled curve while the y-axis on the right is for transition and diffusion-controlled curve. The gradient of these plots gives the rate constant, *k* at each stage.

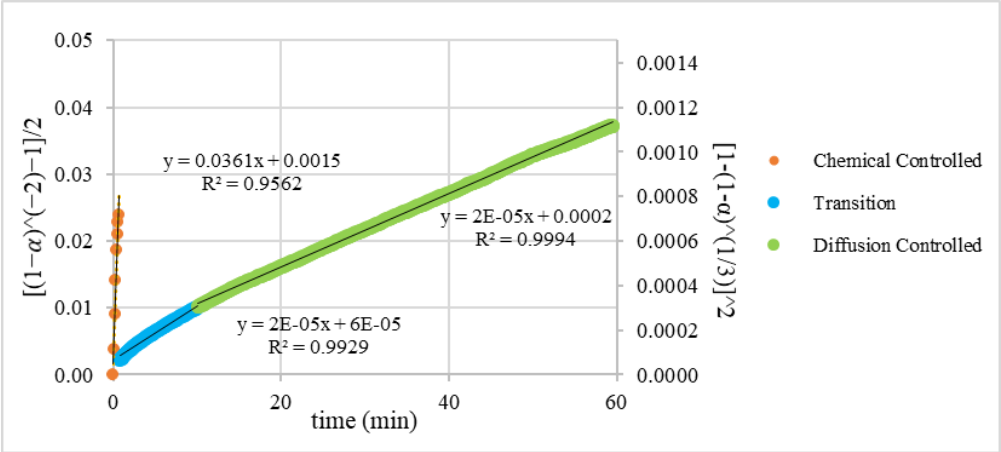

Figure 4.3: Kinetic Plot of CaO at 400 ºC

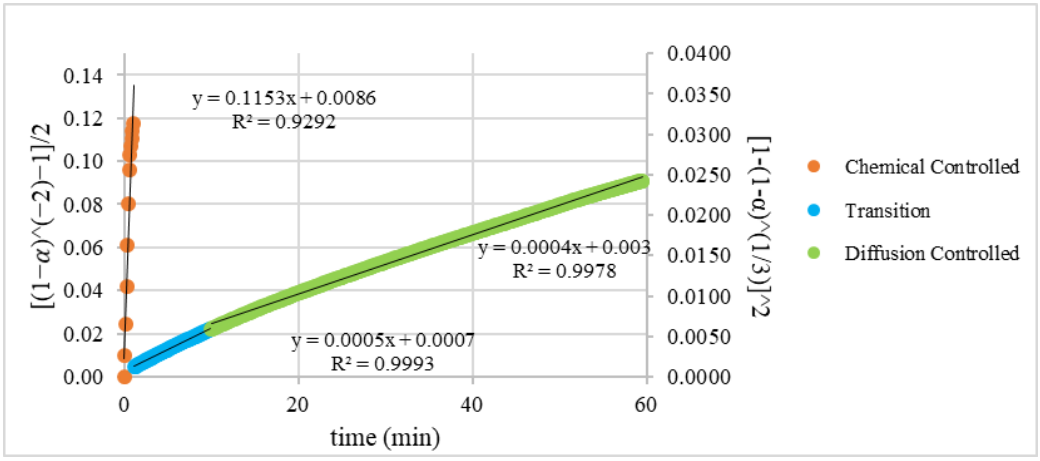

Figure 4.4: Kinetic Plot of CaO at 500 ºC

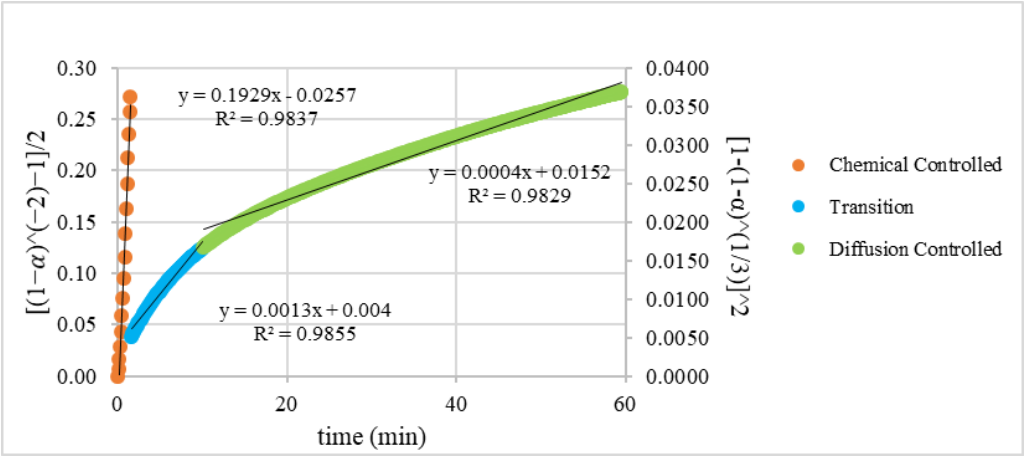

Figure 4.5: Kinetic Plot of CaO at 600 ºC

According to the results, the rate constant, k increases with elevation of temperature. This indicates that CO_2 adsorption reaction favours high temperature (Wei et al., 2017). However, at diffusion-controlled stage, carbonation temperature increase from 500 to 600 ºC does not affect the k value, which means increasing temperature above 500 ºC will not affect the rate at this stage.

Upon obtaining the k value for each stage, *ln(k)* vs *-1/T* was plotted as shown in Figure 4.6. The gradient obtained can be computed into activation energy as displayed in the previous tables. It is known that transition stage and diffusion-controlled stage required higher activation energy than chemical-controlled stage. This is due to more energy is needed to allow the reaction to occur after the formation of $CaCO_3$ layer. More energy is needed to overcome the steric hindrance in order to allow the fresh reactants to contact with each other.

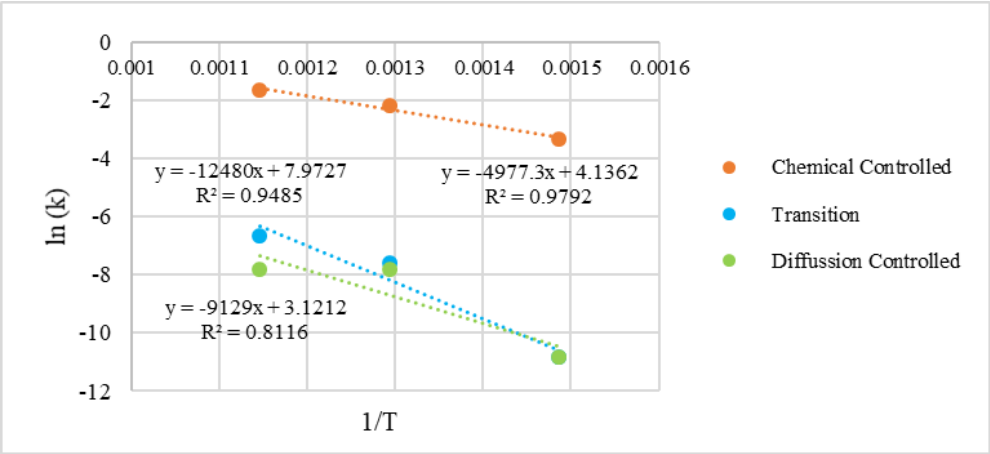

Figure 4.6: Arrhenius Plot of CaO at Each Stage

4.2.2 Kinetic Study for Calcium Oxide-Nickel Oxide Adsorbent

Upon addition of NiO, model fitting was conducted for CaO-NiO, the results obtained for chemical controlled stage is tabulated in Table 4.6, for transition stage is tabulated in Table 4.7 and for diffusion-controlled stage is tabulated in Table 4.8.

Table 4.6: Model fitting of CaO-NiO Adsorbent for Chemical Controlled Stage

Reaction Model	**Carbonation Temperature, *T***	**Rate Constant, k_c (min^{-1})**	**R^2 for *g(α)* vs *t***	**Activation Energy, *E* (J/mol)**	**Pre-exponential factor, *A* (min^{-1})**	**R^2 for *ln(k)* vs *-1/T***
F_0	**400 °C**	**0.0390**	**0.9724**	**58536.38**	**1341.5756**	**0.9993**
	500 °C	**0.1433**	**0.9014**			
	600 °C	**0.4305**	**0.9481**			
F_1	400 °C	0.0415	0.9696	61313.26	2329.2463	0.9987
	500 °C	0.1590	0.9124			
	600 °C	0.5143	0.9481			
F_2	400 °C	0.0441	0.9665	64376.13	4247.5601	0.9980
	500 °C	0.1770	0.9230			
	600 °C	0.6209	0.9457			
F_3	400 °C	0.0470	0.9629	67621.92	8016.8431	0.9970
	500 °C	0.1977	0.9328			
	600 °C	0.7577	0.9407			

Table 4.7: Model fitting of CaO-NiO Adsorbent for Transition Stage

Reaction Model	**Carbonation Temperature, *T***	**Rate Constant, k_t (min^{-1})**	**R^2 for *g(α)* vs *t***	**Activation Energy, *E* (J/mol)**	**Pre-exponential factor, *A* (min^{-1})**	**R^2 for *ln(k)* vs *-1/T***
D_1	400 ºC	0.0030	0.9732	40117.54	4.4584	0.9046
	500 ºC	0.0118	0.9843			
	600 ºC	0.0149	0.9348			
D_2	400 ºC	0.0016	0.9745	45507.51	6.2495	0.9211
	500 ºC	0.0072	0.9883			
	600 ºC	0.0099	0.9436			
D_3	**400 ºC**	**0.0004**	**0.9758**	**50091.85**	**3.4893**	**0.9475**
	500 ºC	**0.0019**	**0.9920**			
	600 ºC	**0.0030**	**0.9527**			
D_4	400 ºC	0.0004	0.9749	44672.78	1.3304	0.9306
	500 ºC	0.0017	0.9896			
	600 ºC	0.0024	0.9468			

Table 4.8: Model fitting of CaO-NiO Adsorbent for Diffusion Controlled Stage

Reaction Model	**Carbonation Temperature, *T***	**Rate Constant, k_d (min^{-1})**	**R^2 for *g(α)* vs *t***	**Activation Energy, *E* (J/mol)**	**Pre-exponential factor, *A* (min^{-1})**	**R^2 for *ln(k)* vs *-1/T***
D_1	400 ºC	0.0011	0.9879	17743.74	0.0293	0.7259
	500 ºC	0.0024	0.9308			
	600 ºC	0.0022	0.9333			
D_2	400 ºC	0.0006	0.9897	26258.94	0.0734	0.8504
	500 ºC	0.0016	0.9379			
	600 ºC	0.0017	0.9397			
D_3	**400 ºC**	**0.0002**	**0.9915**	**27452.00**	**0.0294**	**0.9163**
	500 ºC	**0.0005**	**0.9455**			
	600 ºC	**0.0006**	**0.9468**			
D_4	400 ºC	0.0001	0.9904	35122.49	0.0758	0.8116
	500 ºC	0.0004	0.9405			
	600 ºC	0.0004	0.9422			

At transition stage and diffusion-controlled stage, three-dimensional diffusion Jander Equation (D_3) is the best model to describe the behaviour of CaO-NiO adsorbent. At chemical-controlled stage, zero-order reaction model (F_o) best describes the kinetic behaviour of CaO-NiO adsorbent. Addition of NiO catalyst into CaO adsorbent changed reaction order from three to zero, which means the interaction between NiO and CaO change the course of reaction. If the reaction follows F_0, the rate-determining step is nucleation process (Diefallah et al., 1987). In other words, CO_2 capture process at this stage is identical to the nucleation and growth of crystal, whereby the reaction begins at one point and expand to neighbouring area. Besides, there is equal possibilities of nucleation at each active site.

Figure 4.7, Figure 4.8 and Figure 4.9 shows the plot of $g(\alpha)$ vs t for best fit model at each stage for carbonation temperature of 400, 500 and 600 ºC respectively. The gradient of these plots gives the rate constant, k at each stage.

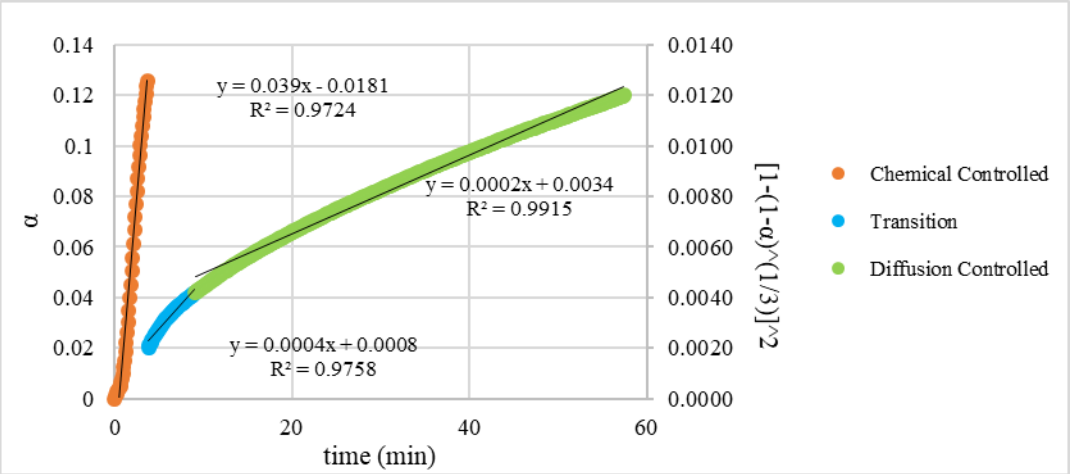

Figure 4.7: Kinetic Plot of CaO-NiO at 400 ºC

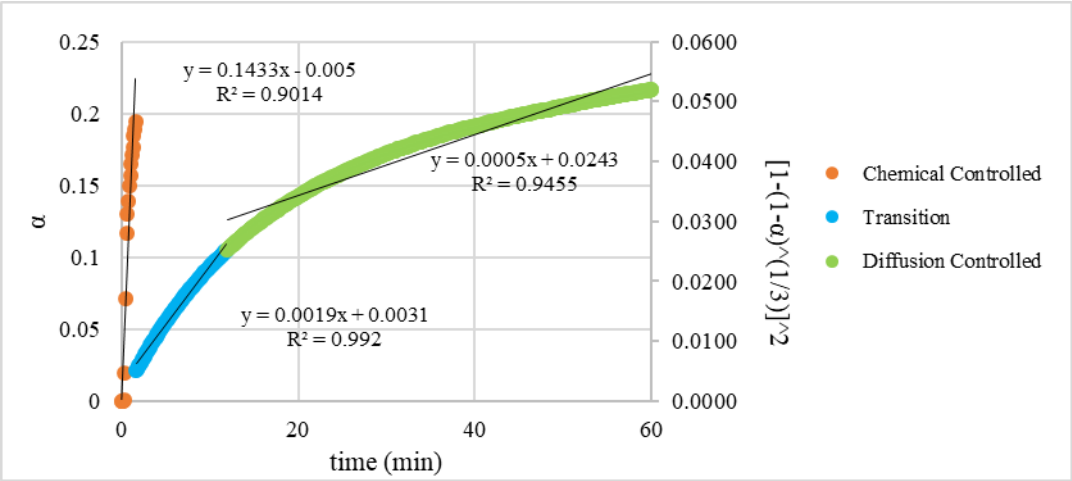

Figure 4.8: Kinetic Plot of CaO-NiO at 500 ºC

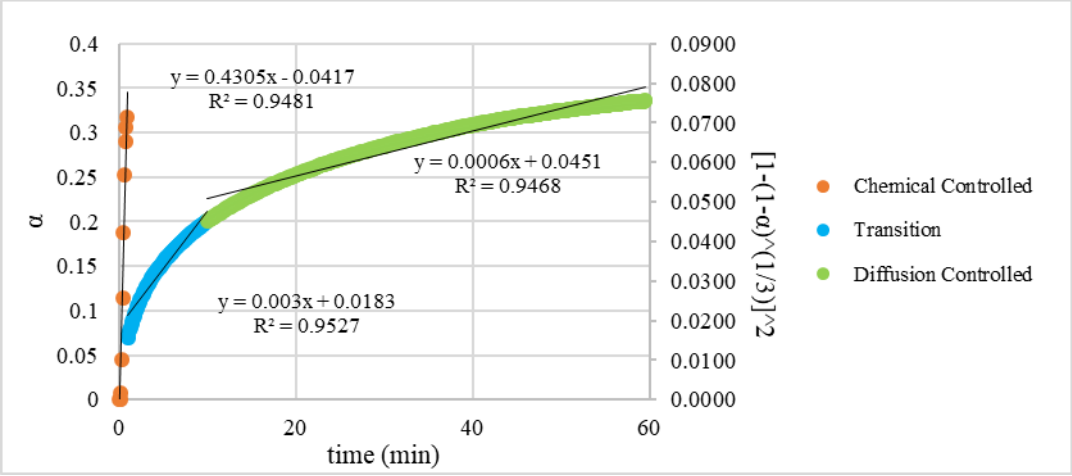

Figure 4.9: Kinetic Plot of CaO-NiO at 600 ºC

According to the results, the same trend was observed for rate constant, where the *k* value increases with temperature. This indicates that CO_2 adsorption reaction favours high temperature despite addition of NiO catalyst. Since the *k* value after addition of NiO catalyst still shows increasing trend with higher temperature, it is hard to conclude whether it will continue increase or remain constant after 600 ºC. Hence, the elevation temperature problem mentioned is still remain unanswered. However, it is confirmed that the *k* value increased after addition of NiO into CaO adsorbent. In other words, introduction of NiO catalyst is able to speed up the rate of adsorption reaction.

Upon obtaining the k value for each stage, *ln(k)* vs *-1/T* was plotted as shown in Figure 4.10. The gradient obtained was computed into activation energy as shown in the previous tables. It is known that addition of NiO cause decrease in activation energy for transition stage and diffusion-controlled stage. This means that presence of NiO is able to aid the diffusion of CO_2 through the $CaCO_3$ formed during chemical controlled stage. Besides, addition of NiO cause increase in activation energy for for chemical-controlled stage. It is suspected that, there might be error in TGA data obtained for CaO adsorbent carbonated at 400 ºC causing the opposite trend to be observed. Hence, it is suggested to redo the TGA study for carbonation temperature of 400 ºC. Pre-exponential factor, *A* is related to collision frequency. *A* in chemical-controlled stage increases significantly after addition of NiO. This means that the rate of CO_2 adsorption is improved with the presence of NiO (Wei et al., 2017).

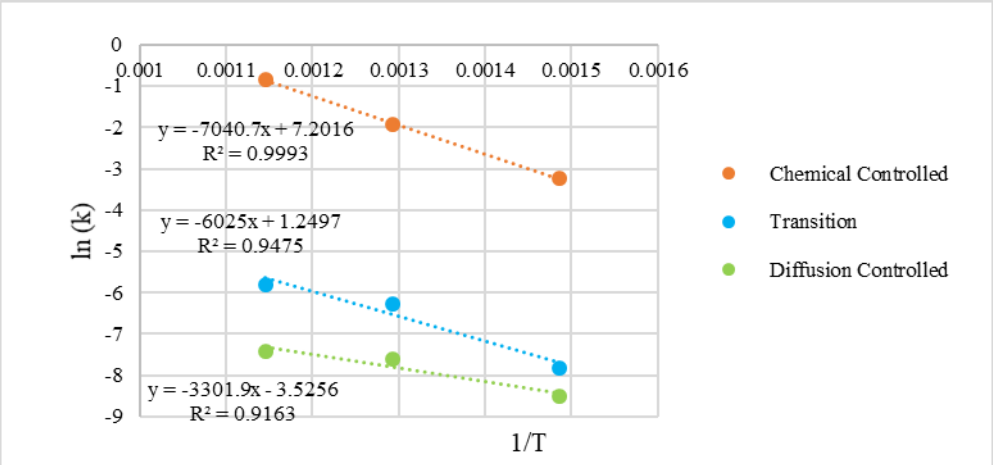

Figure 4.10: Arrhenius Plot of CaO-NiO at Each Stage

In short, it can be concluded that increasing carbonation temperature and presence of NiO catalyst play important role in CO_2 capture process.

4.3 Characterisation of Adsorbent

4.3.1 Scanning Electron Microscope - Energy Dispersive X-ray Analyzer (SEM-EDX)

SEM was used to study the surface morphology of CaO and CaO-NiO adsorbent while EDX was used to determine the surface composition. The SEM images at different conditions were tabulated in Table 4.9.

Table 4.9: SEM Images of Adsorbent with Magnification of x5.5k

	CaO	**CaO-NiO**
Before Carbonation	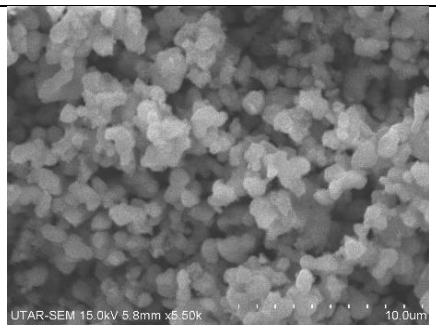	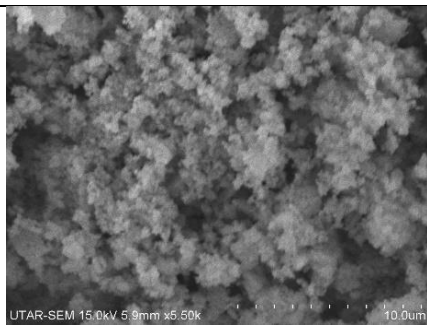
After Carbonation at 400 ºC	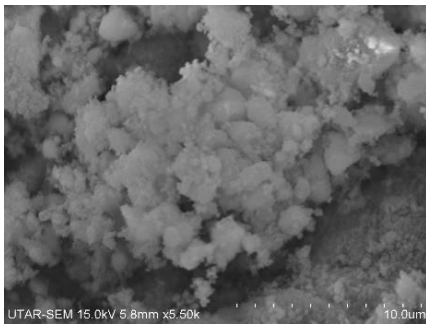	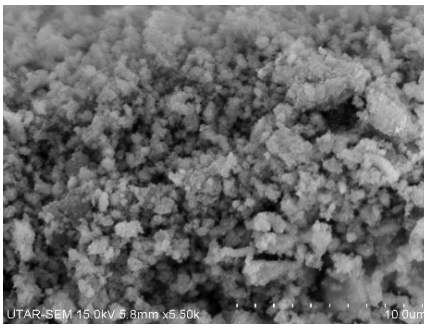
After Carbonation at 500 ºC	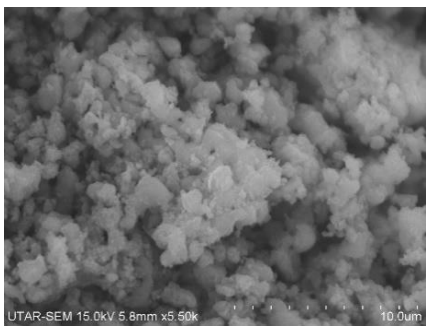	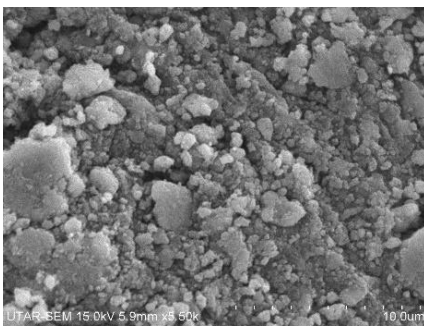
After Carbonation at 600 ºC	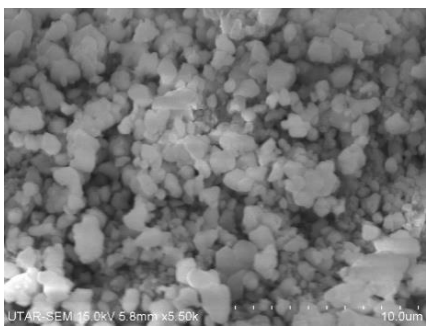	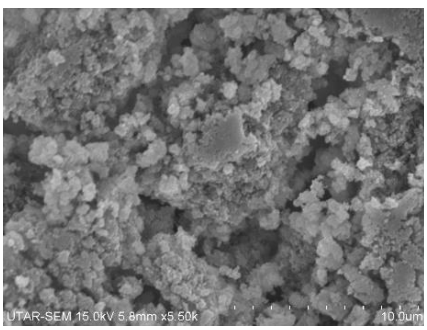

The images obtained showed the surface morphology of adsorbents before and after carbonation. CaO adsorbent before carbonation showed uniform distribution of small octahedral particles. After addition of NiO catalyst, the particle size become smaller and more porous. The porosity dispersed the active sites and allows more CO_2 to attach and react. Hence, CaO-NiO adsorbent is able to give higher capture capacity at chemical reaction-controlled stage compared to pure CaO adsorbent. Besides, the exposure of active site causes less impedance for CO_2 to enter the pores. Hence, the rate of adsorption is increased with presence of NiO.

After carbonation, the adsorbents lost its initial structure due to formation of $CaCO_3$ layer. The formation of $CaCO_3$ further leads to particle size increased, which covers the pores and reduced the porosity of the adsorbent. Besides, agglomeration of particles occurred in the sample. These phenomena were more obvious for sample carbonated at higher temperature as more CO_2 was captured and reacted to form $CaCO_3$ compared to lower carbonation temperature. Parts of the adsorbent remain porous on the surface of the CaO-based sorbents. This means that the spent adsorbent still has potential to capture CO_2 after 60 minutes of carbonation.

Besides, EDX was used to identify the weight percentage of different element presented in the adsorbents. The results from EDX are shown in Table 4.10 and Table 4.11. It is notice that the distribution varies from each tested area, yet the overall distribution of elements at four spots of the adsorbent were even. Besides, the theoretical weight fraction of each adsorbent was computed for comparison purpose as shown in appendix C. Since CaO adsorbent is easily carbonised after synthesising, the weight of $CaCO_3$ is take into consideration for calculation of theoretical weight of CaO sample as well. It is noted that the data for carbon atom is excluded from comparison. This is due to the carbon atom weight percentage will be definitely more than predicted as carbon tape is used to attach the sample on the sample holder. By comparing the fraction computed from EDX data and theoretical data, it is known that the fraction of each atom is similar to predicted value. Hence, sol-gel method is practical for adsorbent synthesis since it is able to provide correct composition for each adsorbent and disperse each atom evenly.

Table 4.10: EDX Results for CaO Adsorbent

	Weight Percentage (wt %)		
Elements	**C**	**O**	**Ca**
Spot 1	11.98	39.39	48.63
Spot 2	22.02	38.84	39.15
Spot 3	28.05	39.13	32.82
Spot 4	25.99	40.47	33.54
Average Distribution	**22.0100**	**39.4575**	**38.5350**
Fraction		0.5059	0.4941
Theoretical Fraction	0.0769	0.4098	0.5133

Table 4.11: EDX Results for CaO-NiO Adsorbent

	Weight Percentage (wt %)			
Elements	**C**	**O**	**Ca**	**Ni**
Spot 1	11.09	28.82	24.91	35.17
Spot 2	5.05	24.59	29.93	40.43
Spot 3	3.78	25.12	32.86	38.25
Spot 4	6.2	24.47	29.43	39.9
Average Distribution	**6.5300**	**25.7500**	**29.2825**	**38.4375**
Fraction		0.2755	0.3133	0.4112
Theoretical Fraction		0.2447	0.3065	0.4488

4.3.2 X-ray Diffraction (XRD)

The XRD results of CaO and CaO-NiO adsorbents are shown in Figure 4.11 and the raw data is shown in appendix D. The primary diffraction peaks for CaO are at 2θ = 28.2º, 31.6º, 32.3º, 36.0º, 37.4º, 53.8º, 64.3º, 64.6º, 65.8º, 67.3º, 67.6º, 79.1º and 79.3º (JCPDS File No.: 00-037-1497), while peaks for NiO are at 2θ =37.3º, 43.3º, 62.9º and 75.3º (JCPDS File No.: 00-047-1049). Besides, peaks for $CaCO_3$ are at 2θ = 23.0º, 23.2º, 29.5º, 36.0º, 39.4º, 43.3º, 43.5º, 47.1º, 47.4º, 47.7º, 48.6º and 57.4º (JCPDS File No.: 00-047-1743).

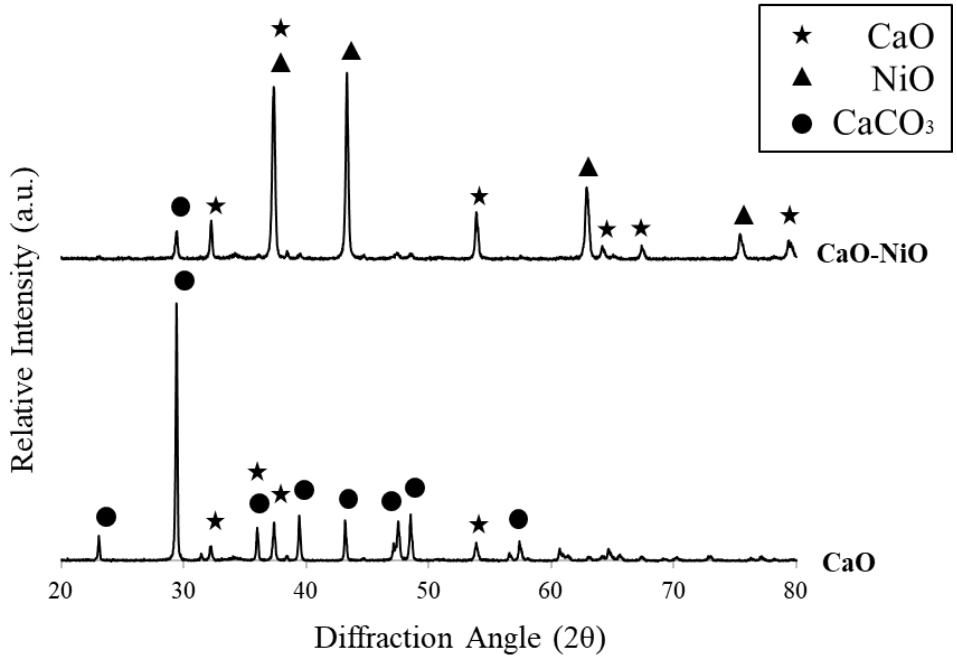

Figure 4.11: X-ray diffraction (XRD) data for CaO and CaO-NiO samples

The XRD spectrum for CaO adsorbent proved the presence of CaO peaks at 2θ = 32.3º, 36.0º, 37.4º and 53.8º. On the other hand, XRD spectrum for CaO-NiO adsorbent contained both CaO peaks at 2θ = 32.3º, 36.0º, 37.4º, 53.8º, 64.3º, 67.3º and 79.3º as well as NiO peaks at 2θ =37.3º, 43.3º, 62.9º and 75.3º. In other words, the adsorbent consisted physical mixtures of CaO and NiO, without presence of mixed metal oxide and solid solution in the adsorbent. Hence, sol-gel method is practical for adsorbent synthesis.

Besides, $CaCO_3$ peaks at 2θ = 23,0º 29.5º, 36.0º, 39.4º, 43.5º, 47.1º, 47.4º, 48.6º and 57.4º were detected in CaO adsorbent while $CaCO_3$ peaks at 2θ = 29.5º

was detected in CaO-NiO adsorbent. This is due to $CaCO_3$ is formed when the adsorbent is cooled during calcination step in adsorbent synthesising process.

Furthermore, the data for three strongest peaks of each adsorbents are displayed in Table 4.12 and Table 4.13. The crystallite size of each adsorbent was computed by using Debye-Scherrer equation. Sample calculation is shown in appendix E. From calculation, it is known that the average crystallite size decreased after addition of NiO. This result confirmed the observation obtained in SEM. Besides, it indicates the addition of NiO will change the crystallographic structure of CaO adsorbent.

Table 4.12: The Data for Three Strongest Peaks for CaO

No.	**Peak No.**	**2 Theta, 2θ (deg)**	**2 Theta, 2θ (rad)**	**Full Width at Half Maximum, *FWHM* (deg)**	**Full Width at Half Maximum, *FWHM* (rad)**	**Crystallite Size, d_x (nm)**
1	2	29.3716	0.5126	0.1413	0.0025	60.7047
2	10	48.4752	0.8461	0.1631	0.0028	55.7907
3	6	39.3960	0.6876	0.1458	0.0025	60.4463
					Average	**58.9806**

Table 4.13: The Data for Three Strongest Peaks for CaO-NiO

No.	**Peak No.**	**2 Theta, 2θ (deg)**	**2 Theta, 2θ (rad)**	**Full Width at Half Maximum, *FWHM* (deg)**	**Full Width at Half Maximum, *FWHM* (rad)**	**Crystallite Size, d_x (nm)**
1	6	43.2698	0.7552	0.2105	0.0037	42.4047
2	4	37.2888	0.6508	0.2610	0.0046	33.5514
3	8	62.8567	1.0971	0.2535	0.0044	38.3587
					Average	**38.1049**

CHAPTER 5

CONCLUSIONS AND RECOMMENDATIONS

5.1 Conclusions

Calcium oxide and calcium oxide-nickel oxide adsorbents were successfully synthesised through sol-gel method. The overall distribution of elements in the sample were even. The fraction of elements obtained from EDX data was similar to theoretical value and XRD showed the presents of each element as predicted. Hence, sol-gel method is practical for adsorbent synthesis. Besides. the CO_2 adsorption capacity curve showed the existence of three regimes including chemical reaction-controlled stage, transition stage, diffusion-controlled stage. The results showed that high adsorption rate and capacity could be achieved at chemically-controlled stage, at higher carbonation temperature as well as by addition of NiO catalyst. The highest adsorption capacity of 0.5661 mg CO_2/ mg CaO as well as highest adsorption rate of 0.3533 mg CO_2/ mg CaO.min was observed on CaO-NiO adsorbent carbonated at 600 ºC. Based on kinetic study, it was found that, the addition of NiO catalyst caused activation energy, E to decrease in transition stage and diffusion-controlled stage as well as cause pre-exponential factor, A to increase in chemical-controlled stage. Based on SEM analysis, particle size become smaller and more porous with presence of NiO catalyst, thus allowing more CO_2 to be captured and reacted. Based on XRD study, addition of NiO decreased the average crystallite size of the adsorbent. In short, these studies conducted indicates that CaO-NiO adsorbent is a better candidate for CO_2 capture compared to pure CaO adsorbent.

5.2 Recommendations for Future Work

As mentioned in previous part, 60 minutes of carbonation might not be sufficient for the adsorbents to be completely carbonise. Hence, longer carbonation study is suggested to allow more comprehensive study. Besides, only carbonation of Calcium Looping Process (CLP) was studied in this project. It is recommended to study the reverse reaction which is calcination to verify the feasibility of CaO-NiO adsorbent in this system. Since, only NiO is used as catalyst in this study, it is suggested to study other transition metal as well. In addition, there are abundance of gas-solid

kinetic models available but only part of the kinetic models was adopted in this research. Hence, more models can be utilised for future studies on CO_2 capture.

REFERENCES

Anthony, E., 2011. Ca looping technology: current status, developments and future directions. Greenhouse Gases: Science and Technology, 1(1), pp.36-47. Ball, D. and Key, J., 2014. *Introductory chemistry*. 1st ed.

Barry Carter, C. and Grant Norton, M., 2007. Sols, Gels, and Organic Chemistry. *Ceramic Materials*, pp.400-411.

Budzianowski, W., 2017. *Energy efficient solvents for CO2 capture by gas-liquid absorption*. Springer International Publishing.

Carbon Capture & Storage Association., n.d.. *What is CCS*. [online] Available at: <http://www.ccsassociation.org/what-is-ccs/> [Accessed 13 Mar. 2018].

Chi, C., Li, Y., Ma, X. and Duan, L., 2017. CO_2 capture performance of CaO modified with by-product of biodiesel at calcium looping conditions. *Chemical Engineering Journal*, 326, pp.378-388.

Diefallah, E., Basahl, S., Obaid, A. and Rafie, A., 1987. Kinetic analysis of thermal decomposition reactions. *Thermochimica Acta*, 111, pp.49-56.

Dunstan, M., Jain, A., Liu, W., Ong, S., Liu, T., Lee, J., Persson, K., Scott, S., Dennis, J. and Grey, C., 2016. Large scale computational screening and experimental discovery of novel materials for high temperature CO2 capture. *Energy & Environmental Science*, 9(4), pp.1346-1360.

Gašparovič, L., Koreňová, Z. and Jelemenský, Ľ., 2010. Kinetic study of wood chips decomposition by TGA. *Chemical Papers*, 64(2).

Guire, M., Hu, M., Gogotsi, Y. and Lu, S., 2004. *Ceramic Nanomaterials and Nanotechnology II*. Westerville, Ohio: The Ameerican Ceramic Society.

Hanak, D., Anthony, E. and Manovic, V., 2015. A review of developments in pilot-plant testing and modelling of calcium looping process for CO_2 capture from power generation systems. *Energy & Environmental Science*, 8(8), pp.2199-2249.

He, S., Hu, Y., Hu, T., Ma, A., Jia, Q., Su, H. and Shan, S., 2017. Investigation of CaO-based sorbents derived from eggshells and red mud for CO_2 capture. *Journal of Alloys and Compounds*, 701, pp.828-833.

Islam, M., Auta, M., Kabir, G. and Hameed, B., 2016. A thermogravimetric analysis of the combustion kinetics of karanja (Pongamia pinnata) fruit hulls char. *Bioresource Technology*, 200, pp.335-341.

Jing, J., Li, T., Zhang, X., Wang, S., Feng, J., Turmel, W. and Li, W., 2017. Enhanced CO_2 sorption performance of CaO/Ca3Al2O6 sorbents and its sintering-resistance mechanism. *Applied Energy*, 199, pp.225-233.

Kanniche, M., Gros-Bonnivard, R., Jaud, P., Valle-Marcos, J., Amann, J. and Bouallou, C., 2010. Pre-combustion, post-combustion and oxy-combustion in thermal power plant for CO_2 capture. *Applied Thermal Engineering*, 30(1), pp.53-62.

Kazi, S., Aranda, A., Meyer, J. and Mastin, J., 2014. High performance CaO-based sorbents for pre- and post- combustion CO2 capture at high temperature. *Energy Procedia*, 63, pp.2207-2215.

Lecomte, F., Broutin, P., Lebas, E., Appert, O. and Jones, T., 2010. *CO_2 capture*. Paris, France: Editions Technip.

Lee, Z., Ichikawa, S., Lee, K. and Mohamed, A., 2015. The role of nickel oxide additive in lowering the carbon dioxide sorption temperature of CaO. *Journal of Energy Chemistry*, 24(2), pp.225-231.

Liu, W., Low, N., Feng, B., Wang, G. and Diniz da Costa, J., 2010. Calcium Precursors for the Production of CaO Sorbents for Multicycle CO_2 Capture. *Environmental Science & Technology*, 44(2), pp.841-847.

Liu, X., Shi, J., He, L., Ma, X. and Xu, S., 2017. Modification of CaO-based sorbents prepared from calcium acetate for CO 2 capture at high temperature. Chinese Journal of Chemical Engineering, 25(5), pp.572-580.

Manovic, V., Anthony, E. and Loncarevic, D., 2009. CO_2 looping cycles with CaO-based sorbent pretreated in CO2 at high temperature. *Chemical Engineering Science*, 64(14), pp.3236-3245.

Maroto-Valer, M., 2010. *Developments and innovation in carbon dioxide capture and storage technology*. North America: Woodhead Publishing Limited.

Martínez, I., Murillo, R., Grasa, G. and Abanades, J., 2011. Integration of a Ca-looping system for CO2 capture in an existing power plant. *Energy Procedia*, 4, pp.1699-1706.

Mokhtar, M., Taib, R. and Hassim, M., 2014. Measurement of PCDD/Fs emissions from a coal–fired power plant in Malaysia and establishment of emission factors. *Atmospheric Pollution Research*, 5(3), pp.388-397.

Nimmas, T., Jamrunroj, P., Wongsakulphasatch, S., Kiatkittipong, W., Laosiripojana, N., Gong, J. and Assabumrungrat, S., 2018. Influence of CaO precursor on CO 2 capture performance and sorption-enhanced steam ethanol reforming. *International Journal of Hydrogen Energy*.

Ortiz, C., Chacartegui, R., Valverde, J. and Becerra, J., 2016. A new integration model of the calcium looping technology into coal fired power plants for CO2 capture. *Applied Energy*, 169, pp.408-420.

Radfarnia, H. and Sayari, A., 2015. A highly efficient CaO-based CO2 sorbent prepared by a citrate-assisted sol–gel technique. *Chemical Engineering Journal*, 262, pp.913-920.

Sivalingam, S., 2013. *CO_2 separation by calcium looping from full and partial fuel oxidation processes*. [online] Stuttgart: Maschinenwesen der Technischen Universität München zur. Available at: <http://www.iaea.org/inis/collection/NCLCollectionStore/_Public/46/031/46031837.pdf> [Accessed 12 Mar. 2018].

Skoufa, Z., Antzara, A., Heracleous, E. and Lemonidou, A., 2016. Evaluating the Activity and Stability of CaO-based Sorbents for Post-combustion CO2 Capture in Fixed-bed Reactor Experiments. *Energy Procedia*, 86, pp.171-180.

Sun, Z., Xu, C., Chen, S. and Xiang, W. (2016). Improvements of CaO-based sorbents for cyclic CO 2 capture using a wet mixing process. *Chemical Engineering Journal*, 286, pp.320-328.

Tomaszewicz, G., Kotyczka-Morańska, M. and Plis, A., 2016. Studies on the carbonation of Czatkowice limestone in Calcium Looping process. *Polish Journal of Chemical Technology*, 18(2), pp.53-58.

United Nations Climate Change., n.d.. *Kyoto Protocol*. [online] Available at: <http://unfccc.int/kyoto_protocol/items/2830.php> [Accessed 12 Mar. 2018].

United States Environmental Protection Agency., n.d.. *Overview of Greenhouse Gases*. [online] Available at: <https://www.epa.gov/ghgemissions/overview-greenhouse-gases> [Accessed 12 Mar. 2018].

Wang, S., Shen, H., Fan, S., Zhao, Y., Ma, X. and Gong, J., 2013. Enhanced CO2adsorption capacity and stability using CaO-based adsorbents treated by hydration. AIChE Journal, 59(10), pp.3586-3593.

Wang, S., Yan, S., Ma, X. and Gong, J., 2011. Recent advances in capture of carbon dioxide using alkali-metal-based oxides. Energy & Environmental Science, 4(10), p.3805.

Wei, M., Yu, Q., Xie, H., Zuo, Z., Hou, L. and Yang, F., 2017. Kinetics studies of CO2 adsorption and desorption on waste ion-exchange resin-based activated carbon. *International Journal of Hydrogen Energy*, 42(44), pp.27122-27129.

Xiang, Z., Liang, J., Morgan, H., Liu, Y., Mao, H. and Bu, Q., 2018. Thermal behavior and kinetic study for co-pyrolysis of lignocellulosic biomass with polyethylene over Cobalt modified ZSM-5 catalyst by thermogravimetric analysis. *Bioresource Technology*, 247, pp.804-811.

Zhang, X. and Cresswell, M., 2016. Materials for Inorganic Controlled Release Technology. *Inorganic Controlled Release Technology*, pp.1-16.

APPENDICES

APPENDIX A: TGA Raw Data

Table A-1: TGA Raw Data for CaO and CaO-NiO Adsorbents at Each Temperature

	Weight of CaO (mg)			Weight of CaO-NiO (mg)		
Time (min)	400 ºC	500 ºC	600 ºC	400 ºC	500 ºC	600 ºC
0.0	14.967	11.144	16.974	17.865	8.881	8.877
0.1	14.956	11.145	16.971	17.865	8.881	8.876
0.2	14.943	11.146	16.968	17.863	8.881	8.875
0.3	14.931	11.148	16.967	17.859	8.884	8.875
0.4	14.926	11.157	16.972	17.854	8.954	8.875
0.5	14.930	11.201	17.012	17.850	9.154	8.874
0.6	14.986	11.308	17.121	17.848	9.324	8.876
0.7	15.063	11.465	17.285	17.849	9.376	8.903
0.8	15.136	11.645	17.482	17.852	9.411	9.045
0.9	15.201	11.826	17.698	17.856	9.450	9.306
1.0	15.235	12.003	17.928	17.863	9.480	9.587
1.1	15.259	12.144	18.172	17.872	9.508	9.837
1.2	15.275	12.200	18.428	17.882	9.531	9.975
1.3	15.290	12.235	18.697	17.893	9.554	10.036
1.4	15.303	12.266	18.973	17.903	9.582	10.084
1.5	15.315	12.295	19.250	17.912	9.600	10.127
1.6	15.326	12.321	19.516	17.918	9.621	10.161
1.7	15.336	12.347	19.767	17.923	9.641	10.193
1.8	15.345	12.371	19.992	17.924	9.659	10.222
1.9	15.354	12.396	20.199	17.924	9.679	10.245
2.0	15.362	12.420	20.325	17.923	9.696	10.268
2.1	15.370	12.444	20.402	17.923	9.714	10.288
2.2	15.378	12.466	20.477	17.922	9.730	10.309
2.3	15.385	12.488	20.544	17.923	9.746	10.327
2.4	15.392	12.511	20.608	17.925	9.762	10.343
2.5	15.399	12.533	20.668	17.929	9.775	10.360
2.6	15.406	12.554	20.725	17.935	9.790	10.376
2.7	15.412	12.575	20.780	17.943	9.804	10.389
2.8	15.419	12.595	20.833	17.950	9.819	10.403
2.9	15.425	12.615	20.885	17.956	9.833	10.417
3.0	15.431	12.635	20.934	17.961	9.844	10.430
3.1	15.437	12.654	20.982	17.967	9.856	10.441
3.2	15.443	12.673	21.030	17.974	9.868	10.452
3.3	15.448	12.693	21.075	17.984	9.880	10.463
3.4	15.453	12.711	21.120	17.997	9.895	10.474

Table A-1 (Continued)

3.5	15.457	12.729	21.163	18.012	9.905	10.486
3.6	15.463	12.746	21.206	18.030	9.917	10.496
3.7	15.467	12.764	21.247	18.052	9.927	10.504
3.8	15.472	12.782	21.287	18.077	9.936	10.514
3.9	15.477	12.799	21.326	18.104	9.947	10.523
4.0	15.482	12.815	21.363	18.135	9.960	10.530
4.1	15.486	12.832	21.401	18.168	9.967	10.539
4.2	15.491	12.848	21.437	18.204	9.979	10.547
4.3	15.495	12.865	21.472	18.242	9.990	10.554
4.4	15.500	12.881	21.507	18.282	9.995	10.562
4.5	15.504	12.897	21.541	18.323	10.005	10.569
4.6	15.508	12.912	21.574	18.364	10.016	10.576
4.7	15.512	12.928	21.607	18.406	10.022	10.581
4.8	15.516	12.943	21.639	18.447	10.033	10.590
4.9	15.521	12.957	21.670	18.488	10.040	10.595
5.0	15.525	12.972	21.700	18.528	10.050	10.601
5.1	15.529	12.986	21.730	18.567	10.057	10.607
5.2	15.533	13.001	21.759	18.604	10.065	10.612
5.3	15.537	13.015	21.788	18.640	10.073	10.619
5.4	15.540	13.029	21.816	18.674	10.083	10.625
5.5	15.544	13.043	21.844	18.706	10.090	10.633
5.6	15.548	13.057	21.870	18.736	10.101	10.637
5.7	15.552	13.070	21.897	18.764	10.104	10.643
5.8	15.555	13.083	21.923	18.791	10.112	10.649
5.9	15.559	13.097	21.949	18.817	10.118	10.654
6.0	15.563	13.110	21.973	18.841	10.127	10.659
6.1	15.566	13.122	21.997	18.864	10.135	10.664
6.2	15.569	13.135	22.021	18.885	10.141	10.669
6.3	15.572	13.148	22.045	18.904	10.148	10.674
6.4	15.575	13.160	22.068	18.923	10.155	10.678
6.5	15.579	13.172	22.091	18.941	10.162	10.683
6.6	15.583	13.184	22.114	18.959	10.168	10.688
6.7	15.586	13.196	22.136	18.975	10.174	10.692
6.8	15.590	13.208	22.158	18.991	10.181	10.696
6.9	15.593	13.220	22.180	19.006	10.188	10.701
7.0	15.597	13.232	22.201	19.020	10.193	10.704
7.1	15.600	13.244	22.221	19.033	10.200	10.709
7.2	15.603	13.255	22.242	19.046	10.206	10.713
7.3	15.606	13.267	22.262	19.058	10.211	10.717
7.4	15.610	13.278	22.283	19.069	10.216	10.721
7.5	15.613	13.289	22.303	19.081	10.223	10.725
7.6	15.615	13.300	22.322	19.091	10.227	10.729
7.7	15.618	13.311	22.341	19.101	10.234	10.733

Table A-1 (Continued)

7.8	15.620	13.323	22.360	19.111	10.240	10.737
7.9	15.623	13.334	22.378	19.120	10.246	10.740
8.0	15.626	13.345	22.395	19.128	10.252	10.743
8.1	15.629	13.355	22.413	19.137	10.257	10.747
8.2	15.633	13.366	22.431	19.145	10.262	10.751
8.3	15.636	13.376	22.448	19.153	10.267	10.754
8.4	15.639	13.386	22.465	19.161	10.273	10.758
8.5	15.642	13.397	22.482	19.168	10.278	10.761
8.6	15.645	13.407	22.499	19.175	10.283	10.765
8.7	15.647	13.417	22.515	19.182	10.289	10.769
8.8	15.650	13.427	22.532	19.189	10.292	10.772
8.9	15.653	13.437	22.549	19.195	10.297	10.775
9.0	15.655	13.447	22.565	19.202	10.303	10.778
9.1	15.658	13.457	22.581	19.208	10.307	10.781
9.2	15.661	13.467	22.595	19.214	10.311	10.783
9.3	15.664	13.477	22.610	19.220	10.317	10.787
9.4	15.667	13.487	22.625	19.226	10.323	10.791
9.5	15.669	13.496	22.640	19.232	10.327	10.793
9.6	15.672	13.506	22.654	19.237	10.332	10.796
9.7	15.674	13.516	22.669	19.242	10.335	10.798
9.8	15.677	13.525	22.683	19.248	10.340	10.802
9.9	15.680	13.535	22.697	19.253	10.344	10.805
10.0	15.682	13.545	22.711	19.258	10.349	10.807
10.1	15.685	13.554	22.726	19.263	10.354	10.810
10.2	15.687	13.563	22.740	19.268	10.357	10.813
10.3	15.690	13.573	22.753	19.273	10.361	10.816
10.4	15.692	13.581	22.766	19.278	10.365	10.820
10.5	15.695	13.590	22.779	19.283	10.369	10.822
10.6	15.698	13.599	22.792	19.288	10.372	10.824
10.7	15.701	13.608	22.805	19.292	10.377	10.827
10.8	15.704	13.617	22.818	19.297	10.381	10.830
10.9	15.706	13.626	22.831	19.301	10.384	10.832
11.0	15.708	13.635	22.844	19.306	10.389	10.834
11.1	15.711	13.644	22.856	19.310	10.392	10.836
11.2	15.713	13.652	22.869	19.314	10.395	10.839
11.3	15.716	13.661	22.881	19.319	10.400	10.840
11.4	15.719	13.669	22.893	19.323	10.403	10.844
11.5	15.721	13.678	22.904	19.326	10.407	10.847
11.6	15.724	13.686	22.916	19.331	10.412	10.849
11.7	15.726	13.695	22.927	19.335	10.416	10.852
11.8	15.729	13.703	22.939	19.339	10.420	10.853
11.9	15.731	13.712	22.950	19.343	10.422	10.855
12.0	15.734	13.720	22.961	19.347	10.425	10.857

Table A-1 (Continued)

12.1	15.736	13.728	22.973	19.351	10.430	10.860
12.2	15.738	13.736	22.984	19.356	10.432	10.863
12.3	15.741	13.744	22.995	19.360	10.436	10.865
12.4	15.743	13.752	23.006	19.364	10.439	10.868
12.5	15.745	13.760	23.017	19.368	10.443	10.869
12.6	15.748	13.769	23.027	19.372	10.447	10.871
12.7	15.750	13.777	23.038	19.376	10.451	10.873
12.8	15.752	13.786	23.048	19.380	10.452	10.876
12.9	15.754	13.794	23.058	19.384	10.456	10.877
13.0	15.756	13.802	23.069	19.387	10.460	10.879
13.1	15.758	13.810	23.079	19.391	10.462	10.881
13.2	15.761	13.818	23.089	19.395	10.466	10.883
13.3	15.763	13.825	23.099	19.399	10.468	10.887
13.4	15.765	13.833	23.109	19.403	10.471	10.889
13.5	15.768	13.841	23.118	19.406	10.475	10.890
13.6	15.770	13.848	23.128	19.410	10.478	10.892
13.7	15.772	13.855	23.138	19.414	10.481	10.893
13.8	15.774	13.863	23.147	19.418	10.484	10.895
13.9	15.776	13.870	23.157	19.421	10.487	10.898
14.0	15.778	13.878	23.166	19.425	10.490	10.899
14.1	15.780	13.885	23.175	19.429	10.493	10.901
14.2	15.782	13.893	23.184	19.432	10.497	10.902
14.3	15.784	13.900	23.193	19.436	10.498	10.905
14.4	15.787	13.907	23.203	19.439	10.501	10.907
14.5	15.789	13.915	23.212	19.443	10.504	10.910
14.6	15.792	13.922	23.221	19.446	10.506	10.911
14.7	15.794	13.929	23.230	19.449	10.510	10.913
14.8	15.797	13.936	23.238	19.453	10.511	10.914
14.9	15.799	13.943	23.247	19.456	10.514	10.916
15.0	15.801	13.951	23.256	19.459	10.517	10.918
15.1	15.803	13.958	23.264	19.462	10.519	10.919
15.2	15.805	13.966	23.273	19.465	10.523	10.921
15.3	15.806	13.973	23.281	19.468	10.526	10.922
15.4	15.808	13.980	23.289	19.472	10.528	10.924
15.5	15.810	13.987	23.297	19.475	10.530	10.926
15.6	15.812	13.993	23.305	19.478	10.532	10.928
15.7	15.814	14.000	23.313	19.481	10.534	10.929
15.8	15.816	14.007	23.321	19.484	10.538	10.931
15.9	15.818	14.013	23.329	19.488	10.540	10.932
16.0	15.819	14.020	23.338	19.491	10.544	10.935
16.1	15.821	14.026	23.345	19.494	10.546	10.937
16.2	15.823	14.033	23.353	19.497	10.548	10.938
16.3	15.825	14.039	23.361	19.500	10.550	10.940

Table A-1 (Continued)

16.4	15.827	14.046	23.369	19.503	10.552	10.941
16.5	15.829	14.052	23.377	19.506	10.555	10.942
16.6	15.831	14.059	23.385	19.509	10.556	10.945
16.7	15.832	14.065	23.393	19.512	10.559	10.946
16.8	15.834	14.071	23.400	19.514	10.561	10.947
16.9	15.835	14.077	23.407	19.517	10.563	10.949
17.0	15.836	14.083	23.415	19.520	10.565	10.952
17.1	15.838	14.090	23.422	19.522	10.569	10.953
17.2	15.839	14.096	23.429	19.525	10.570	10.954
17.3	15.841	14.102	23.437	19.528	10.572	10.955
17.4	15.843	14.109	23.444	19.531	10.575	10.957
17.5	15.846	14.115	23.451	19.534	10.577	10.959
17.6	15.848	14.121	23.459	19.536	10.579	10.960
17.7	15.850	14.126	23.466	19.539	10.580	10.963
17.8	15.851	14.132	23.473	19.542	10.583	10.964
17.9	15.853	14.138	23.480	19.545	10.586	10.965
18.0	15.854	14.144	23.486	19.547	10.588	10.966
18.1	15.855	14.149	23.493	19.550	10.590	10.967
18.2	15.857	14.155	23.500	19.553	10.592	10.968
18.3	15.859	14.161	23.506	19.556	10.595	10.969
18.4	15.860	14.167	23.513	19.558	10.597	10.971
18.5	15.862	14.172	23.520	19.561	10.598	10.972
18.6	15.864	14.178	23.528	19.563	10.600	10.975
18.7	15.865	14.184	23.534	19.566	10.602	10.976
18.8	15.866	14.190	23.541	19.569	10.604	10.977
18.9	15.868	14.196	23.548	19.571	10.606	10.978
19.0	15.869	14.202	23.555	19.574	10.608	10.980
19.1	15.871	14.208	23.561	19.576	10.610	10.981
19.2	15.873	14.213	23.568	19.579	10.613	10.982
19.3	15.874	14.219	23.574	19.582	10.615	10.984
19.4	15.876	14.224	23.581	19.584	10.616	10.985
19.5	15.878	14.230	23.587	19.587	10.618	10.986
19.6	15.880	14.236	23.593	19.590	10.620	10.987
19.7	15.882	14.241	23.600	19.592	10.621	10.988
19.8	15.883	14.247	23.606	19.594	10.622	10.989
19.9	15.885	14.252	23.611	19.597	10.625	10.990
20.0	15.886	14.258	23.617	19.599	10.628	10.992
20.1	15.888	14.264	23.623	19.602	10.629	10.994
20.2	15.889	14.269	23.629	19.604	10.631	10.995
20.3	15.891	14.274	23.636	19.607	10.632	10.995
20.4	15.893	14.280	23.642	19.609	10.634	10.997
20.5	15.895	14.284	23.648	19.612	10.636	10.998
20.6	15.896	14.290	23.655	19.614	10.638	11.000

Table A-1 (Continued)

20.7	15.898	14.295	23.661	19.616	10.639	11.001
20.8	15.900	14.301	23.667	19.618	10.642	11.003
20.9	15.901	14.306	23.673	19.620	10.644	11.004
21.0	15.903	14.311	23.679	19.623	10.645	11.004
21.1	15.905	14.317	23.685	19.625	10.647	11.006
21.2	15.906	14.322	23.691	19.627	10.648	11.007
21.3	15.908	14.328	23.696	19.630	10.650	11.008
21.4	15.909	14.333	23.702	19.632	10.652	11.010
21.5	15.911	14.338	23.708	19.634	10.653	11.012
21.6	15.912	14.343	23.714	19.637	10.655	11.012
21.7	15.914	14.348	23.719	19.639	10.658	11.012
21.8	15.915	14.353	23.725	19.642	10.660	11.013
21.9	15.917	14.358	23.731	19.644	10.661	11.015
22.0	15.918	14.363	23.736	19.646	10.662	11.017
22.1	15.919	14.368	23.742	19.648	10.663	11.018
22.2	15.921	14.374	23.748	19.651	10.665	11.018
22.3	15.923	14.379	23.753	19.653	10.668	11.019
22.4	15.924	14.384	23.759	19.655	10.669	11.020
22.5	15.926	14.389	23.764	19.657	10.671	11.021
22.6	15.927	14.394	23.769	19.659	10.672	11.022
22.7	15.929	14.399	23.775	19.662	10.674	11.024
22.8	15.930	14.405	23.780	19.664	10.675	11.025
22.9	15.932	14.409	23.785	19.666	10.676	11.026
23.0	15.933	14.415	23.791	19.668	10.678	11.027
23.1	15.935	14.419	23.796	19.671	10.679	11.028
23.2	15.936	14.425	23.802	19.673	10.679	11.030
23.3	15.938	14.429	23.807	19.675	10.680	11.032
23.4	15.940	14.434	23.812	19.677	10.682	11.032
23.5	15.941	14.439	23.817	19.679	10.683	11.033
23.6	15.943	14.444	23.823	19.681	10.686	11.034
23.7	15.945	14.449	23.828	19.684	10.687	11.035
23.8	15.947	14.454	23.833	19.686	10.689	11.037
23.9	15.948	14.459	23.838	19.688	10.690	11.038
24.0	15.950	14.464	23.843	19.691	10.692	11.038
24.1	15.952	14.469	23.848	19.692	10.693	11.039
24.2	15.954	14.474	23.853	19.694	10.694	11.040
24.3	15.955	14.479	23.859	19.696	10.695	11.041
24.4	15.957	14.484	23.865	19.698	10.696	11.042
24.5	15.959	14.488	23.870	19.700	10.697	11.044
24.6	15.960	14.493	23.875	19.702	10.699	11.045
24.7	15.962	14.497	23.880	19.704	10.700	11.046
24.8	15.963	14.501	23.886	19.706	10.702	11.046
24.9	15.965	14.506	23.890	19.709	10.703	11.048

Table A-1 (Continued)

25.0	15.966	14.511	23.895	19.711	10.705	11.048
25.1	15.968	14.516	23.900	19.712	10.707	11.049
25.2	15.969	14.520	23.905	19.714	10.709	11.049
25.3	15.971	14.525	23.910	19.716	10.709	11.052
25.4	15.973	14.529	23.914	19.719	10.711	11.052
25.5	15.975	14.533	23.920	19.721	10.712	11.053
25.6	15.976	14.538	23.925	19.723	10.713	11.055
25.7	15.977	14.543	23.930	19.725	10.714	11.055
25.8	15.978	14.547	23.935	19.727	10.715	11.056
25.9	15.980	14.552	23.940	19.729	10.716	11.057
26.0	15.982	14.557	23.945	19.731	10.718	11.058
26.1	15.983	14.561	23.949	19.733	10.719	11.059
26.2	15.985	14.566	23.954	19.735	10.720	11.060
26.3	15.986	14.570	23.959	19.737	10.721	11.060
26.4	15.987	14.575	23.964	19.739	10.722	11.061
26.5	15.988	14.580	23.968	19.741	10.723	11.063
26.6	15.990	14.584	23.973	19.743	10.725	11.063
26.7	15.991	14.588	23.978	19.745	10.726	11.063
26.8	15.993	14.593	23.982	19.746	10.727	11.065
26.9	15.995	14.597	23.987	19.748	10.729	11.066
27.0	15.996	14.602	23.992	19.750	10.732	11.066
27.1	15.998	14.606	23.996	19.752	10.732	11.066
27.2	15.999	14.610	24.001	19.754	10.732	11.068
27.3	16.001	14.614	24.006	19.756	10.733	11.069
27.4	16.002	14.618	24.010	19.758	10.734	11.069
27.5	16.004	14.623	24.015	19.760	10.735	11.070
27.6	16.005	14.627	24.019	19.762	10.737	11.071
27.7	16.007	14.631	24.024	19.764	10.738	11.072
27.8	16.009	14.636	24.028	19.766	10.740	11.074
27.9	16.010	14.640	24.033	19.768	10.740	11.074
28.0	16.012	14.645	24.037	19.770	10.741	11.074
28.1	16.013	14.649	24.042	19.772	10.743	11.075
28.2	16.014	14.654	24.046	19.774	10.744	11.077
28.3	16.016	14.658	24.051	19.776	10.745	11.078
28.4	16.017	14.662	24.055	19.778	10.746	11.078
28.5	16.019	14.666	24.060	19.779	10.747	11.079
28.6	16.020	14.670	24.064	19.781	10.748	11.080
28.7	16.021	14.674	24.069	19.783	10.749	11.081
28.8	16.023	14.679	24.073	19.784	10.750	11.082
28.9	16.024	14.683	24.078	19.786	10.752	11.083
29.0	16.026	14.688	24.082	19.788	10.753	11.084
29.1	16.027	14.692	24.086	19.790	10.754	11.085
29.2	16.028	14.696	24.091	19.792	10.754	11.085

Table A-1 (Continued)

29.3	16.030	14.700	24.095	19.794	10.756	11.086
29.4	16.031	14.704	24.099	19.795	10.756	11.087
29.5	16.032	14.709	24.103	19.797	10.757	11.088
29.6	16.034	14.713	24.108	19.799	10.759	11.089
29.7	16.035	14.717	24.112	19.800	10.760	11.089
29.8	16.036	14.721	24.116	19.802	10.762	11.089
29.9	16.037	14.725	24.120	19.804	10.763	11.091
30.0	16.038	14.729	24.125	19.806	10.764	11.092
30.1	16.039	14.733	24.129	19.808	10.765	11.092
30.2	16.041	14.737	24.134	19.810	10.766	11.093
30.3	16.042	14.741	24.138	19.811	10.767	11.093
30.4	16.043	14.745	24.143	19.813	10.768	11.094
30.5	16.045	14.749	24.147	19.814	10.769	11.094
30.6	16.046	14.754	24.152	19.816	10.769	11.095
30.7	16.047	14.758	24.155	19.818	10.770	11.096
30.8	16.049	14.762	24.159	19.819	10.771	11.097
30.9	16.050	14.766	24.164	19.820	10.772	11.099
31.0	16.052	14.769	24.168	19.821	10.772	11.100
31.1	16.053	14.773	24.173	19.823	10.775	11.101
31.2	16.054	14.777	24.177	19.825	10.776	11.102
31.3	16.056	14.781	24.181	19.827	10.777	11.102
31.4	16.057	14.785	24.185	19.828	10.777	11.103
31.5	16.059	14.789	24.189	19.830	10.777	11.104
31.6	16.061	14.793	24.193	19.832	10.778	11.104
31.7	16.062	14.797	24.197	19.834	10.779	11.105
31.8	16.063	14.801	24.201	19.835	10.781	11.106
31.9	16.065	14.804	24.205	19.837	10.782	11.107
32.0	16.066	14.808	24.209	19.838	10.782	11.107
32.1	16.066	14.812	24.213	19.840	10.783	11.107
32.2	16.068	14.816	24.217	19.841	10.783	11.108
32.3	16.069	14.820	24.221	19.843	10.784	11.109
32.4	16.071	14.824	24.225	19.846	10.786	11.109
32.5	16.073	14.828	24.229	19.847	10.787	11.109
32.6	16.074	14.832	24.232	19.849	10.787	11.110
32.7	16.076	14.836	24.236	19.851	10.788	11.111
32.8	16.078	14.840	24.240	19.853	10.789	11.111
32.9	16.079	14.844	24.244	19.854	10.789	11.112
33.0	16.080	14.848	24.248	19.855	10.791	11.113
33.1	16.081	14.851	24.252	19.857	10.792	11.114
33.2	16.082	14.855	24.256	19.858	10.793	11.115
33.3	16.083	14.858	24.260	19.860	10.795	11.115
33.4	16.085	14.862	24.264	19.861	10.796	11.116
33.5	16.087	14.866	24.268	19.863	10.797	11.117

Table A-1 (Continued)

33.6	16.088	14.870	24.272	19.864	10.797	11.118
33.7	16.089	14.874	24.276	19.866	10.797	11.117
33.8	16.091	14.878	24.280	19.867	10.797	11.118
33.9	16.092	14.882	24.284	19.869	10.798	11.119
34.0	16.093	14.885	24.287	19.871	10.799	11.120
34.1	16.094	14.889	24.291	19.873	10.800	11.121
34.2	16.095	14.893	24.295	19.874	10.801	11.122
34.3	16.096	14.896	24.299	19.876	10.802	11.122
34.4	16.098	14.900	24.303	19.878	10.802	11.123
34.5	16.099	14.905	24.306	19.880	10.803	11.124
34.6	16.100	14.908	24.311	19.881	10.803	11.124
34.7	16.102	14.912	24.314	19.882	10.804	11.125
34.8	16.103	14.915	24.318	19.884	10.805	11.126
34.9	16.104	14.919	24.321	19.885	10.807	11.126
35.0	16.106	14.922	24.325	19.887	10.809	11.127
35.1	16.107	14.926	24.328	19.889	10.809	11.128
35.2	16.108	14.930	24.332	19.890	10.809	11.128
35.3	16.109	14.933	24.336	19.892	10.809	11.128
35.4	16.110	14.936	24.340	19.894	10.810	11.129
35.5	16.111	14.940	24.344	19.895	10.811	11.129
35.6	16.112	14.943	24.348	19.897	10.812	11.130
35.7	16.114	14.947	24.351	19.898	10.813	11.131
35.8	16.115	14.951	24.355	19.900	10.813	11.131
35.9	16.117	14.954	24.358	19.901	10.815	11.133
36.0	16.118	14.958	24.362	19.902	10.816	11.134
36.1	16.119	14.962	24.366	19.904	10.816	11.136
36.2	16.120	14.965	24.370	19.905	10.816	11.136
36.3	16.122	14.969	24.373	19.907	10.817	11.136
36.4	16.123	14.972	24.377	19.908	10.818	11.136
36.5	16.125	14.975	24.381	19.910	10.818	11.136
36.6	16.126	14.978	24.384	19.912	10.820	11.136
36.7	16.128	14.982	24.388	19.913	10.821	11.137
36.8	16.129	14.986	24.392	19.915	10.822	11.137
36.9	16.130	14.989	24.395	19.917	10.822	11.138
37.0	16.131	14.993	24.398	19.918	10.822	11.139
37.1	16.132	14.996	24.402	19.919	10.824	11.140
37.2	16.133	15.000	24.406	19.921	10.824	11.141
37.3	16.134	15.003	24.409	19.922	10.825	11.141
37.4	16.135	15.007	24.413	19.924	10.826	11.142
37.5	16.136	15.010	24.416	19.925	10.826	11.143
37.6	16.138	15.013	24.420	19.926	10.826	11.143
37.7	16.139	15.017	24.424	19.928	10.826	11.143
37.8	16.140	15.020	24.428	19.930	10.827	11.144

Table A-1 (Continued)

37.9	16.142	15.023	24.431	19.932	10.828	11.145
38.0	16.143	15.027	24.435	19.933	10.829	11.145
38.1	16.144	15.030	24.438	19.935	10.829	11.146
38.2	16.145	15.034	24.442	19.936	10.830	11.147
38.3	16.147	15.037	24.445	19.938	10.831	11.147
38.4	16.148	15.041	24.449	19.939	10.831	11.147
38.5	16.149	15.044	24.453	19.940	10.833	11.148
38.6	16.150	15.048	24.457	19.942	10.834	11.149
38.7	16.151	15.051	24.460	19.943	10.835	11.149
38.8	16.153	15.054	24.464	19.945	10.835	11.150
38.9	16.154	15.057	24.467	19.946	10.835	11.150
39.0	16.155	15.060	24.471	19.947	10.835	11.151
39.1	16.157	15.063	24.474	19.948	10.836	11.151
39.2	16.158	15.067	24.477	19.950	10.837	11.152
39.3	16.159	15.070	24.481	19.951	10.837	11.153
39.4	16.160	15.073	24.484	19.953	10.837	11.155
39.5	16.161	15.077	24.488	19.954	10.838	11.155
39.6	16.162	15.080	24.491	19.956	10.839	11.156
39.7	16.163	15.083	24.494	19.957	10.839	11.156
39.8	16.164	15.086	24.498	19.959	10.839	11.156
39.9	16.165	15.089	24.501	19.960	10.840	11.156
40.0	16.166	15.093	24.504	19.961	10.841	11.156
40.1	16.167	15.096	24.508	19.963	10.842	11.156
40.2	16.169	15.100	24.511	19.964	10.843	11.157
40.3	16.170	15.104	24.515	19.965	10.843	11.158
40.4	16.171	15.107	24.518	19.966	10.843	11.158
40.5	16.172	15.110	24.521	19.967	10.844	11.159
40.6	16.173	15.113	24.525	19.968	10.844	11.159
40.7	16.174	15.116	24.528	19.969	10.844	11.159
40.8	16.176	15.119	24.531	19.971	10.845	11.160
40.9	16.177	15.122	24.535	19.972	10.846	11.161
41.0	16.178	15.126	24.538	19.973	10.847	11.162
41.1	16.179	15.129	24.541	19.975	10.848	11.162
41.2	16.180	15.132	24.545	19.977	10.849	11.163
41.3	16.182	15.136	24.548	19.978	10.850	11.164
41.4	16.183	15.139	24.551	19.980	10.851	11.165
41.5	16.184	15.142	24.553	19.982	10.851	11.166
41.6	16.185	15.146	24.556	19.983	10.852	11.165
41.7	16.186	15.149	24.559	19.985	10.852	11.165
41.8	16.188	15.152	24.563	19.986	10.851	11.166
41.9	16.189	15.155	24.566	19.987	10.852	11.167
42.0	16.191	15.158	24.570	19.989	10.853	11.167
42.1	16.192	15.162	24.573	19.990	10.854	11.167

Table A-1 (Continued)

42.2	16.193	15.165	24.576	19.991	10.855	11.167
42.3	16.195	15.168	24.579	19.992	10.855	11.167
42.4	16.196	15.171	24.582	19.993	10.856	11.168
42.5	16.197	15.174	24.585	19.994	10.857	11.168
42.6	16.198	15.177	24.589	19.996	10.857	11.169
42.7	16.200	15.180	24.592	19.997	10.857	11.169
42.8	16.201	15.184	24.595	19.999	10.858	11.170
42.9	16.202	15.187	24.598	20.000	10.858	11.171
43.0	16.203	15.190	24.601	20.002	10.859	11.171
43.1	16.204	15.193	24.604	20.003	10.861	11.171
43.2	16.204	15.196	24.607	20.004	10.861	11.172
43.3	16.206	15.198	24.611	20.005	10.861	11.173
43.4	16.207	15.201	24.614	20.006	10.862	11.174
43.5	16.208	15.203	24.617	20.007	10.862	11.174
43.6	16.210	15.206	24.620	20.009	10.863	11.173
43.7	16.211	15.210	24.623	20.010	10.864	11.174
43.8	16.211	15.213	24.626	20.012	10.864	11.174
43.9	16.213	15.216	24.630	20.013	10.864	11.175
44.0	16.214	15.219	24.633	20.014	10.866	11.176
44.1	16.215	15.223	24.636	20.016	10.866	11.177
44.2	16.216	15.226	24.639	20.017	10.866	11.177
44.3	16.217	15.229	24.642	20.018	10.868	11.177
44.4	16.218	15.232	24.645	20.019	10.868	11.178
44.5	16.219	15.236	24.648	20.020	10.868	11.179
44.6	16.221	15.239	24.650	20.022	10.869	11.179
44.7	16.222	15.242	24.654	20.023	10.869	11.179
44.8	16.223	15.245	24.657	20.024	10.870	11.179
44.9	16.225	15.248	24.660	20.026	10.870	11.180
45.0	16.226	15.251	24.663	20.027	10.870	11.180
45.1	16.227	15.254	24.665	20.028	10.871	11.181
45.2	16.228	15.257	24.668	20.029	10.871	11.181
45.3	16.230	15.260	24.671	20.030	10.872	11.182
45.4	16.231	15.263	24.674	20.032	10.873	11.182
45.5	16.233	15.266	24.677	20.033	10.874	11.182
45.6	16.234	15.269	24.680	20.035	10.874	11.183
45.7	16.235	15.272	24.683	20.036	10.874	11.184
45.8	16.236	15.275	24.687	20.037	10.874	11.183
45.9	16.237	15.278	24.690	20.039	10.875	11.184
46.0	16.238	15.282	24.693	20.040	10.875	11.185
46.1	16.240	15.285	24.695	20.041	10.876	11.185
46.2	16.241	15.288	24.698	20.042	10.877	11.185
46.3	16.242	15.291	24.700	20.043	10.877	11.185
46.4	16.243	15.294	24.703	20.045	10.877	11.185

Table A-1 (Continued)

46.5	16.244	15.298	24.705	20.046	10.878	11.186
46.6	16.246	15.301	24.709	20.047	10.879	11.186
46.7	16.247	15.304	24.712	20.048	10.880	11.186
46.8	16.248	15.307	24.715	20.050	10.880	11.187
46.9	16.250	15.309	24.718	20.051	10.881	11.186
47.0	16.251	15.312	24.721	20.052	10.882	11.187
47.1	16.253	15.315	24.724	20.053	10.882	11.188
47.2	16.255	15.318	24.727	20.054	10.882	11.188
47.3	16.256	15.321	24.730	20.056	10.882	11.189
47.4	16.257	15.324	24.732	20.057	10.882	11.190
47.5	16.259	15.327	24.735	20.058	10.883	11.190
47.6	16.260	15.330	24.738	20.060	10.884	11.190
47.7	16.261	15.333	24.741	20.061	10.885	11.190
47.8	16.262	15.337	24.744	20.062	10.885	11.190
47.9	16.262	15.341	24.747	20.063	10.885	11.190
48.0	16.264	15.344	24.750	20.064	10.886	11.191
48.1	16.265	15.347	24.753	20.066	10.885	11.192
48.2	16.266	15.349	24.755	20.067	10.886	11.192
48.3	16.268	15.352	24.758	20.068	10.886	11.192
48.4	16.269	15.355	24.760	20.069	10.886	11.193
48.5	16.270	15.358	24.763	20.070	10.887	11.193
48.6	16.271	15.361	24.766	20.071	10.889	11.193
48.7	16.272	15.364	24.769	20.072	10.889	11.194
48.8	16.273	15.367	24.771	20.074	10.888	11.195
48.9	16.274	15.370	24.774	20.075	10.890	11.194
49.0	16.275	15.373	24.777	20.076	10.891	11.195
49.1	16.276	15.376	24.779	20.078	10.892	11.196
49.2	16.277	15.379	24.782	20.079	10.892	11.196
49.3	16.279	15.383	24.785	20.080	10.892	11.196
49.4	16.280	15.386	24.788	20.081	10.892	11.197
49.5	16.281	15.389	24.790	20.081	10.892	11.197
49.6	16.282	15.392	24.793	20.082	10.893	11.197
49.7	16.283	15.395	24.795	20.083	10.893	11.198
49.8	16.284	15.398	24.798	20.084	10.894	11.199
49.9	16.285	15.400	24.801	20.085	10.894	11.199
50.0	16.287	15.403	24.804	20.086	10.894	11.198
50.1	16.288	15.406	24.806	20.087	10.895	11.199
50.2	16.289	15.409	24.809	20.088	10.895	11.200
50.3	16.291	15.412	24.812	20.090	10.896	11.201
50.4	16.292	15.415	24.814	20.091	10.897	11.201
50.5	16.293	15.418	24.817	20.092	10.897	11.202
50.6	16.294	15.421	24.819	20.094	10.898	11.202
50.7	16.294	15.424	24.822	20.095	10.898	11.202

Table A-1 (Continued)

50.8	16.295	15.427	24.825	20.096	10.899	11.202
50.9	16.296	15.430	24.827	20.098	10.899	11.202
51.0	16.297	15.433	24.830	20.099	10.900	11.201
51.1	16.298	15.436	24.833	20.100	10.899	11.202
51.2	16.299	15.439	24.835	20.100	10.900	11.203
51.3	16.299	15.442	24.837	20.101	10.901	11.203
51.4	16.300	15.445	24.840	20.103	10.901	11.203
51.5	16.301	15.447	24.843	20.104	10.902	11.204
51.6	16.302	15.450	24.846	20.105	10.902	11.204
51.7	16.303	15.453	24.848	20.105	10.904	11.205
51.8	16.304	15.456	24.850	20.106	10.905	11.205
51.9	16.305	15.459	24.853	20.107	10.905	11.205
52.0	16.306	15.463	24.855	20.108	10.905	11.205
52.1	16.307	15.466	24.857	20.109	10.905	11.205
52.2	16.308	15.468	24.859	20.110	10.905	11.206
52.3	16.308	15.471	24.862	20.111	10.905	11.206
52.4	16.309	15.473	24.864	20.113	10.906	11.207
52.5	16.310	15.476	24.867	20.114	10.907	11.207
52.6	16.311	15.478	24.870	20.115	10.907	11.207
52.7	16.312	15.481	24.873	20.116	10.908	11.208
52.8	16.313	15.484	24.876	20.117	10.908	11.208
52.9	16.314	15.487	24.878	20.119	10.908	11.208
53.0	16.314	15.490	24.881	20.120	10.909	11.208
53.1	16.315	15.492	24.883	20.121	10.910	11.208
53.2	16.316	15.495	24.885	20.122	10.910	11.208
53.3	16.317	15.498	24.888	20.122	10.910	11.208
53.4	16.318	15.500	24.891	20.124	10.911	11.209
53.5	16.319	15.503	24.894	20.125	10.911	11.210
53.6	16.319	15.505	24.897	20.127	10.911	11.210
53.7	16.320	15.508	24.900	20.128	10.911	11.211
53.8	16.321	15.510	24.902	20.129	10.912	11.212
53.9	16.321	15.513	24.904	20.130	10.912	11.212
54.0	16.322	15.516	24.906	20.131	10.913	11.212
54.1	16.323	15.518	24.909	20.132	10.913	11.212
54.2	16.324	15.521	24.911	20.133	10.914	11.213
54.3	16.325	15.524	24.914	20.134	10.914	11.213
54.4	16.326	15.527	24.917	20.135	10.914	11.213
54.5	16.327	15.529	24.919	20.137	10.914	11.213
54.6	16.328	15.531	24.922	20.138	10.914	11.214
54.7	16.329	15.534	24.924	20.139	10.916	11.214
54.8	16.330	15.536	24.927	20.140	10.917	11.214
54.9	16.331	15.538	24.929	20.141	10.918	11.214
55.0	16.331	15.541	24.932	20.142	10.919	11.214

Table A-1 (Continued)

55.1	16.332	15.544	24.934	20.144	10.919	11.214
55.2	16.332	15.546	24.936	20.145	10.919	11.214
55.3	16.333	15.549	24.939	20.146	10.919	11.214
55.4	16.334	15.551	24.941	20.147	10.919	11.215
55.5	16.335	15.553	24.944	20.148	10.919	11.215
55.6	16.336	15.556	24.946	20.149	10.920	11.214
55.7	16.338	15.558	24.948	20.150	10.921	11.215
55.8	16.339	15.561	24.951	20.151	10.921	11.216
55.9	16.340	15.564	24.953	20.152	10.921	11.217
56.0	16.341	15.566	24.955	20.153	10.921	11.218
56.1	16.342	15.568	24.957	20.154	10.922	11.217
56.2	16.342	15.571	24.960	20.155	10.922	11.217
56.3	16.344	15.573	24.962	20.156	10.924	11.217
56.4	16.345	15.575	24.965	20.157	10.924	11.218
56.5	16.345	15.578	24.967	20.158	10.923	11.219
56.6	16.346	15.581	24.970	20.159	10.923	11.219
56.7	16.347	15.583	24.972	20.160	10.923	11.219
56.8	16.348	15.585	24.975	20.161	10.925	11.219
56.9	16.349	15.587	24.977	20.162	10.925	11.220
57.0	16.350	15.589	24.980	20.164	10.925	11.220
57.1	16.351	15.592	24.982	20.164	10.927	11.220
57.2	16.352	15.594	24.985	20.165	10.926	11.221
57.3	16.353	15.597	24.987	20.166	10.926	11.221
57.4	16.354	15.599	24.990	20.167	10.926	11.221
57.5	16.356	15.602	24.992	20.168	10.927	11.221
57.6	16.357	15.604	24.994	20.169	10.928	11.221
57.7	16.358	15.607	24.997	20.171	10.927	11.221
57.8	16.359	15.610	24.999	20.172	10.927	11.221
57.9	16.359	15.612	25.001	20.173	10.927	11.221
58.0	16.360	15.615	25.004	20.174	10.928	11.222
58.1	16.361	15.617	25.006	20.175	10.929	11.223
58.2	16.362	15.619	25.008	20.176	10.929	11.224
58.3	16.363	15.621	25.011	20.177	10.930	11.224
58.4	16.364	15.623	25.014	20.178	10.930	11.225
58.5	16.365	15.625	25.016	20.180	10.931	11.225
58.6	16.366	15.628	25.019	20.181	10.931	11.225
58.7	16.368	15.630	25.022	20.182	10.932	11.225
58.8	16.368	15.633	25.024	20.183	10.933	11.225
58.9	16.369	15.635	25.026	20.184	10.933	11.225
59.0	16.370	15.638	25.028	20.185	10.933	11.225
59.1	16.370	15.640	25.029	20.186	10.935	11.225
59.2	16.372	15.642	25.032	20.187	10.935	11.226
59.3	16.373	15.645	25.034	20.188	10.935	11.226

Table A-1 (Continued)

59.4	16.374	15.647	25.036	20.188	10.935	11.227
59.5	16.375	15.650	25.038	20.189	10.935	11.227
59.6	16.376	15.652	25.041	20.191	10.935	11.226
59.7	16.376	15.654	25.043	20.192	10.936	11.226
59.8	16.377	15.656	25.046	20.193	10.937	11.227
59.9	16.377	15.658	25.048	20.193	10.938	11.228
60.0	16.378	15.661	25.051	20.195	10.938	11.228

APPENDIX B: Calculation of Adsorption Rate and Capacity

The data for CaO-NiO adsorbent carbonated at 500 ºC and at chemically controlled stage are shown below.

m(0) = 8.881 mg

m(t) = m (1.6 min) = 9.621 mg

t = 1.6 min

Adsorption rate can be calculated based on Eq. 3.1.

$$CO_2\ adsorption\ rate\ = \frac{m(t) - m(0)}{m(0) \times f_{CaO} \times t}$$

where

m(0) = mass of adsorbent at time 0 (mg)

m(t) = mass of adsorbent at time t (mg)

f_{CaO} = mass fraction of CaO in adsorbent

t = time (min)

$$f_{CaO} = \frac{0.5\ \text{mol} \times 56.0774\ \frac{\text{g}}{\text{mol}}}{0.5\ \text{mol} \times 56.0774\ \frac{\text{g}}{\text{mol}} + 0.5\ \text{mol} \times \frac{74.6928\text{g}}{\text{mol}}}$$

$$= 0.4288$$

$$CO_2\ adsorption\ rate\ = \frac{9.621\ \text{mg} - \ 8.881\ \text{mg}}{8.881\ \text{mg} \times 0.4288 \times 1.6\ min}$$

$$= 0.1214\ mg\ CO_2/\ mg\ CaO.min$$

Adsorption capacity can be calculated based on Eq. 3.2

$$CO_2\ adsorption\ capacity\ = \alpha\ = \frac{m(t) - m(0)}{m(0) \times f_{CaO}}$$

where

α = conversion

m(0) = mass of adsorbent at time 0 (mg)

m(t) = mass of adsorbent at time t (mg)

f_{CaO} = mass fraction of CaO in adsorbent

$$CO_2\ adsorption\ capacity = \alpha\ = \frac{9.621\ \text{mg} - \ 8.881\ \text{mg}}{8.881\ \text{mg} \times 0.4288}$$

$$= 0.1943\ mg\ \ CO_2 / mg\ CaO$$

APPENDIX C: Calculation for EDX

Theoretical mass fraction of CaO

Since $CaCO_3$ forms rapidly during cooling of sample, the mass of CaO adsorbent is calculated as total mass of CaO and $CaCO_3$ mixture in 1 mol basis.

$$Mass\ of\ CaO\ and\ CaCO_3$$
$$= 2\ mol \times 40.078 \frac{g}{mol} + 1\ mol \times 12.0107 \frac{g}{mol} + 4\ mol \times 15.9994 \frac{g}{mol}$$
$$= 156.1643\ g$$

$$Mass\ fraction\ of\ Ca = \frac{2\ mol \times 40.078 \frac{g}{mol}}{156.1643\ g} = 0.5133$$

$$Mass\ fraction\ of\ C = \frac{1\ mol \times 12.0107 \frac{g}{mol}}{156.1643\ g} = 0.0769$$

$$Mass\ fraction\ of\ O = \frac{4\ mol \times 15.9994 \frac{g}{mol}}{156.1643\ g} = 0.4098$$

Theoretical mass fraction of CaO-NiO.

Since CaO and NiO has molar ratio of 1 to 1, the mass of CaO-NiO adsorbent is calculated as shown below.

$$Mass\ of\ CaO - NiO$$
$$= 0.5\ mol \times 40.078 \frac{g}{mol} + 0.5\ mol \times 58.6934 \frac{g}{mol} + 2 \times 0.5\ mol \times 15.9994 \frac{g}{mol}$$
$$= 63.3851\ g$$

$$Mass\ fraction\ of\ Ca = \frac{0.5\ mol \times 40.078 \frac{g}{mol}}{63.3851\ g} = 0.3065$$

$$Mass\ fraction\ of\ C = \frac{0.5\ mol \times 58.6934 \frac{g}{mol}}{63.3851\ g} = 0.4488$$

$$Mass\ fraction\ of\ O = \frac{2 \times 0.5\ mol \times 15.9994 \frac{g}{mol}}{63.3851\ g} = 0.2447$$

APPENDIX D: XRD Raw Data

*** Basic Data Process ***

Group : LeeZhiHua
Data : CaO_NEW

Strongest 3 peaks

no.	peak no.	2Theta (deg)	d (A)	I/I1	FWHM (deg)	Intensity (Counts)	Integrated Int (Counts)
1	2	29.3716	3.03844	100	0.14130	1550	12910
2	10	48.4752	1.87639	19	0.16310	296	2795
3	6	39.3960	2.28533	19	0.14580	292	2509

Peak Data List

peak no.	2Theta (deg)	d (A)	I/I1	FWHM (deg)	Intensity (Counts)	Integrated Int (Counts)
1	23.0316	3.85848	8	0.14330	130	1116
2	29.3716	3.03844	100	0.14130	1550	12910
3	32.1650	2.78065	5	0.19000	84	931
4	35.9596	2.49545	13	0.15220	198	1689
5	37.3142	2.40791	14	0.19430	221	2417
6	39.3960	2.28533	19	0.14580	292	2509
7	43.1476	2.09492	17	0.13520	265	2068
8	47.1006	1.92790	6	0.15870	92	932
9	47.4661	1.91390	16	0.18990	241	2583
10	48.4752	1.87639	19	0.16310	296	2795
11	53.8199	1.70198	7	0.22380	104	1273
12	56.5531	1.62604	3	0.14260	52	430
13	57.3855	1.60442	8	0.15890	131	1250
14	60.6652	1.52529	5	0.16420	82	1006
15	64.6548	1.44047	5	0.16500	77	760

```
         ***  Basic Data Process  ***

# Data Infomation
          Group               : LeeZhiHua
          Data                : CaO_NEW
          Sample Nmae         : CaO_NEW
          Comment             :
          Date & Time         : 07-23-18 09:14:51

# Measurement Condition
    X-ray tube
          target              : Cu
          voltage             : 40.0 (kV)
          current             : 30.0 (mA)
    Slits
          Auto Slit           : not Used
          divergence slit     :   1.00000 (deg)
          scatter slit        :   1.00000 (deg)
          receiving slit      :   0.30000(mm)
    Scanning
          drive axis          : Theta-2Theta
          scan range          :   20.0000 - 80.0000 (deg)
          scan mode           : Continuous Scan
          scan speed          :    2.0000 (deg/min)
          sampling pitch      :    0.0200 (deg)
          preset time         :    0.60 (sec)

# Data Process Condition
    Smoothing                 [ AUTO ]
          smoothing points    : 9
    B.G.Subtruction           [ AUTO ]
          sampling points     : 9
          repeat times        : 30
    Ka1-a2 Separate           [ MANUAL ]
          Ka1 a2 ratio        : 50 (%)
    Peak Search               [ AUTO ]
          differential points : 9
          FWHM threhold       : 0.050 (deg)
          intensity threhold  : 30 (par mil)
          FWHM ratio  (n-1)/n : 2
    System error Correction   [ NO ]
    Precise peak Correction   [ NO ]
```

< Group: LeeZhiHua Data: CaO_NEW >

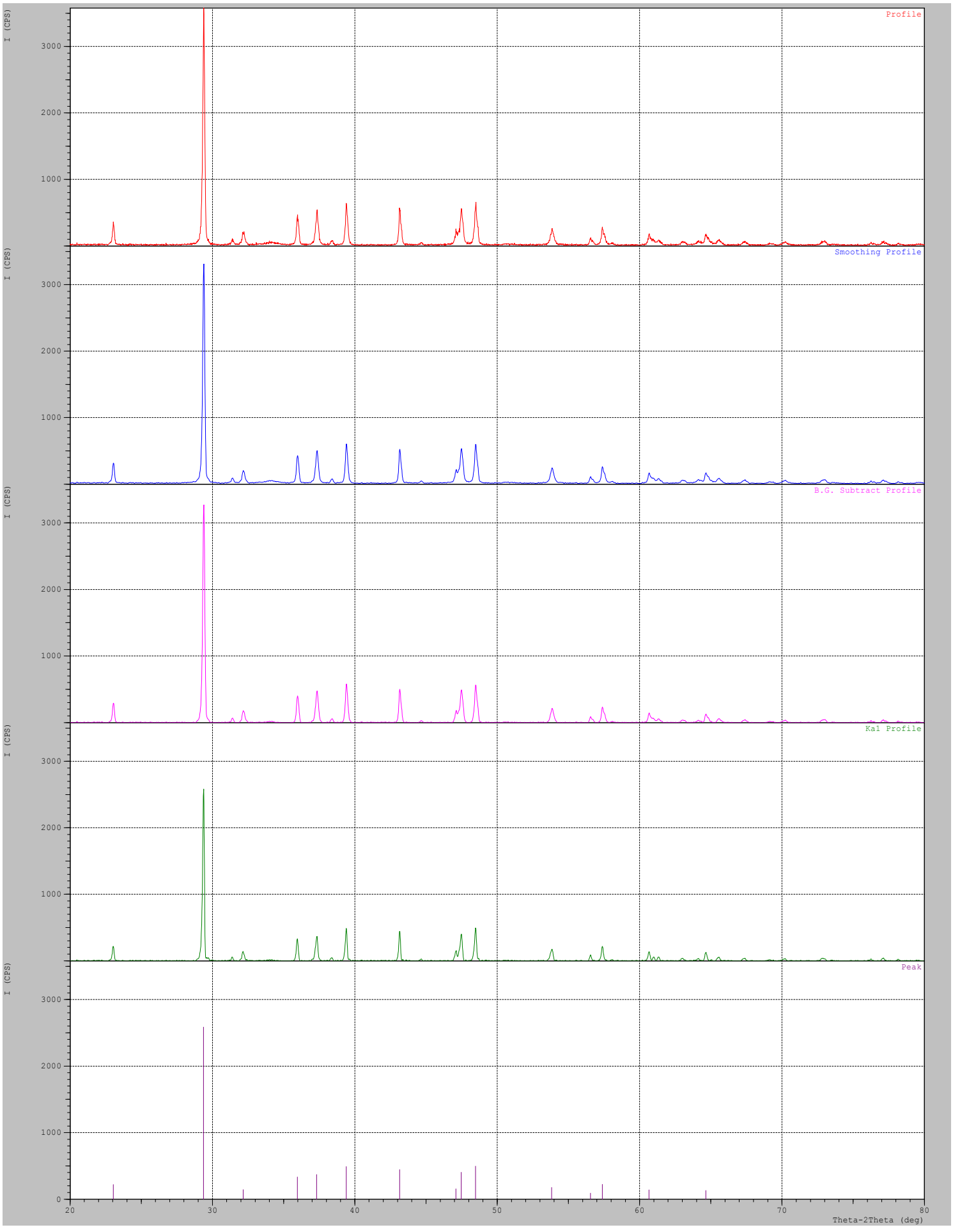

*** Basic Data Process ***

Group : LeeZhiHua
Data : CaONiO_NEW

Strongest 3 peaks

no.	peak no.	2Theta (deg)	d (A)	I/I1	FWHM (deg)	Intensity (Counts)	Integrated Int (Counts)
1	6	43.2698	2.08928	100	0.21050	1137	14297
2	4	37.2888	2.40949	90	0.26100	1020	14892
3	8	62.8567	1.47728	43	0.25350	490	7501

Peak Data List

peak no.	2Theta (deg)	d (A)	I/I1	FWHM (deg)	Intensity (Counts)	Integrated Int (Counts)
1	29.3616	3.03945	13	0.21590	151	1910
2	32.1931	2.77829	19	0.19260	212	2416
3	36.8400	2.43781	3	0.11420	35	353
4	37.2888	2.40949	90	0.26100	1020	14892
5	38.3900	2.34287	3	0.16000	39	392
6	43.2698	2.08928	100	0.21050	1137	14297
7	53.8493	1.70112	27	0.20870	308	3814
8	62.8567	1.47728	43	0.25350	490	7501
9	64.1335	1.45091	7	0.22300	79	1121
10	67.3700	1.38886	7	0.24660	80	1116
11	75.3823	1.25989	16	0.25260	181	2864
12	79.3694	1.20630	11	0.27710	120	2147

```
         ***  Basic Data Process  ***

# Data Infomation
          Group               : LeeZhiHua
          Data                : CaONiO_NEW
          Sample Nmae         : CaONiO_NEW
          Comment             :
          Date & Time         : 07-23-18 09:51:11

# Measurement Condition
    X-ray tube
          target              : Cu
          voltage             : 40.0 (kV)
          current             : 30.0 (mA)
    Slits
          Auto Slit           : not Used
          divergence slit     :   1.00000 (deg)
          scatter slit        :   1.00000 (deg)
          receiving slit      :   0.30000(mm)
    Scanning
          drive axis          : Theta-2Theta
          scan range          :   20.0000 - 80.0000 (deg)
          scan mode           : Continuous Scan
          scan speed          :    2.0000 (deg/min)
          sampling pitch      :    0.0200 (deg)
          preset time         :    0.60 (sec)

# Data Process Condition
    Smoothing                 [ AUTO ]
          smoothing points    : 13
    B.G.Subtruction           [ AUTO ]
          sampling points     : 15
          repeat times        : 30
    Ka1-a2 Separate           [ MANUAL ]
          Ka1 a2 ratio        : 50 (%)
    Peak Search               [ AUTO ]
          differential points : 11
          FWHM threhold       : 0.050 (deg)
          intensity threhold  : 30 (par mil)
          FWHM ratio  (n-1)/n : 2
    System error Correction   [ NO ]
    Precise peak Correction   [ NO ]
```

< Group: LeeZhiHua Data: CaONiO_NEW >

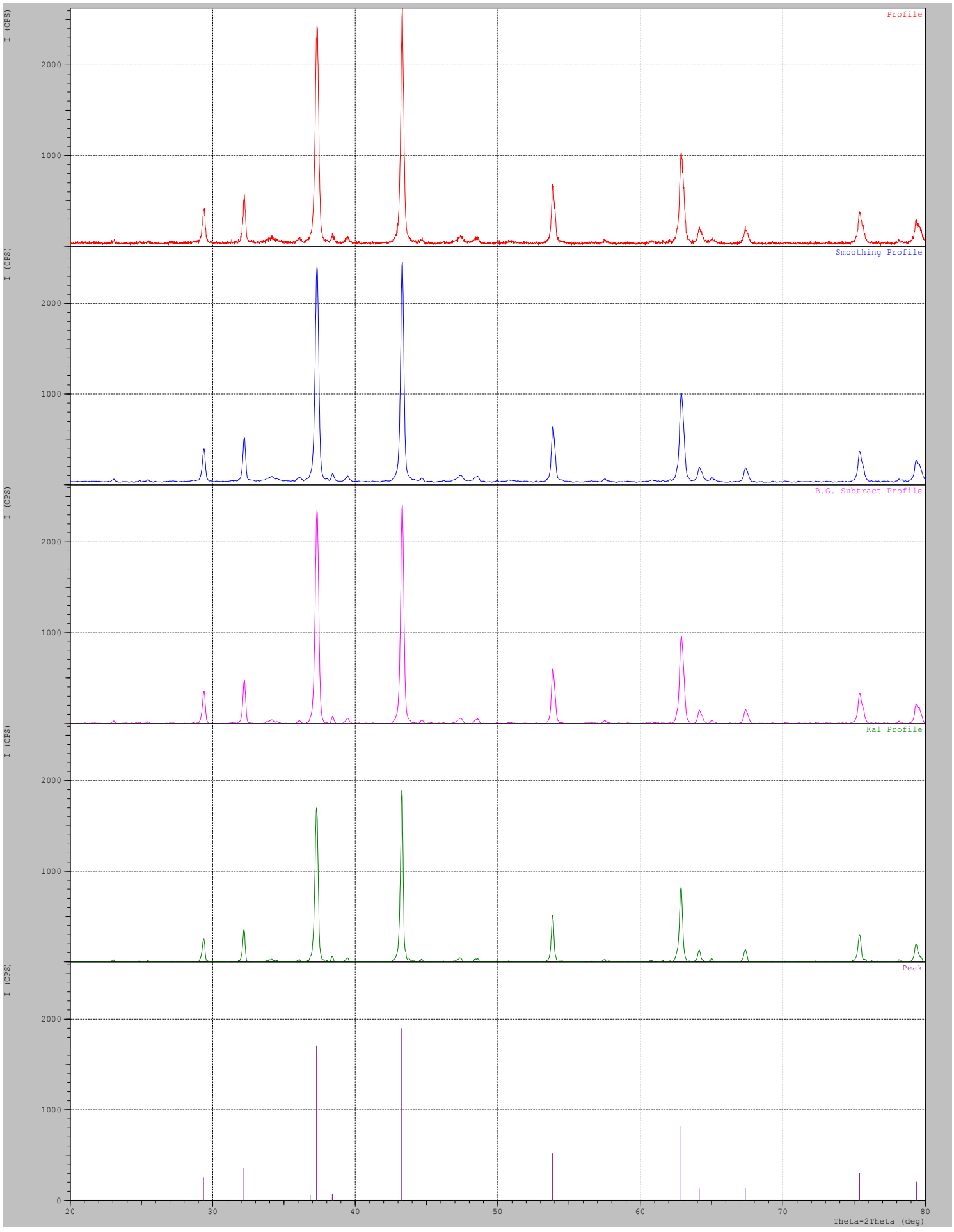

APPENDIX E: Calculation for XRD

Crystallite size of materials can be calculated from XRD raw data with the aid of Scherrer's equation (Guire et al., 2004),

$$d_x = \frac{0.94\lambda}{FWHM.cos\theta}$$

where

d_x = Crystallite size, nm

λ = wavelength of X−ray = 0.15406nm (CuKα)

$FWHM$ = Full Width at Half Maximum, rad

θ = Bragg angle, rad

Data from CaO, peak number 6 was used for sample calculation. The XRD data are as follow:

2 Theta, 2θ =39.3960 º

Full Width at Half Maximum, $FWHM$ = 0.1458 º

Convert 2 Theta from degree to radian,

$$2\ \text{Theta}, 2\theta = 39.3960° \times \frac{\pi}{180°}$$
$$= 0.6876\ \text{rad}$$

Convert Full Width at Half Maximum from degree to radian,

$$\text{Full Width at Half Maximum, FWHM} = 0.1458° \times \frac{\pi}{180°}$$
$$= 0.0025\ \text{rad}$$

Calculate crystallite size by using Scherrer's equation,

$$Crystallite\ size, d_x = \frac{0.94\lambda}{FWHM.cos\theta}$$
$$= \frac{0.94(0.15406\text{nm})}{(0.0025\ \text{rad}).\cos\left(\frac{0.6876\ \text{rad}}{2}\right)}$$
$$= 60.4463\ nm$$